

FINAL REPORT  
FATIGUE STUDY OF A GRP PEDESTRIAN BRIDGE

by

Fred C. McCormick  
Faculty Research Scientist

(The opinions, findings, and conclusions expressed in this report are those of the author and not necessarily those of the sponsoring agencies.)

Virginia Highway & Transportation Research Council  
(A Cooperative Organization Sponsored Jointly by the Virginia  
Department of Highways & Transportation and  
the University of Virginia)

In Cooperation with the U. S. Department of Transportation  
Federal Highway Administration

Charlottesville, Virginia

December 1986  
VHTRC 87-R7

## BRIDGE RESEARCH ADVISORY COMMITTEE

- L. L. MISENHEIMER, Chairman, District Structure & Bridge Engineer, VDOT  
J. E. ANDREWS, Structural Engineer Supervisor, VDOT  
G. W. BOYKIN, District Materials Engineer, VDOT  
C. L. CHAMBERS, Division Bridge Engineer, FHWA  
C. D. GARVER, JR., Division Administrator -- Construction Div., VDOT  
M. H. HILTON, Senior Research Scientist, VTRC  
J. G. G. MCGEE, Assistant Construction Engineer, VDOT  
M. F. MENEFEY, JR., Structural Steel Engineer, VDOT  
R. H. MORECOCK, District Structure & Bridge Engineer, VDOT  
C. A. NASH, JR., District Engineer, VDOT  
F. L. PREWOZNIK, District Structure & Bridge Engineer, VDOT  
W. L. SELLARS, District Structure & Bridge Engineer, VDOT  
F. G. SUTHERLAND, State Structure & Bridge Engineer, VDOT  
L. R. L. WANG, Prof. of Civil Engineering, Old Dominion University

## TABLE OF CONTENTS

	Page
LIST OF FIGURES.....	v
ABSTRACT.....	vii
INTRODUCTION.....	1
PURPOSE AND SCOPE.....	2
EXPERIMENTAL TEST CRITERIA AND PROCEDURES.....	3
Transverse Load Distribution.....	3
Cyclic Load Sequences.....	5
Ultimate Static Load.....	5
Monitoring Instrumentation.....	9
TEST RESULTS.....	10
Transverse Load Distribution.....	11
Cyclic Load Tests.....	13
Load Series 1.....	14
Load Series 2 through 5.....	18
Load Series 6 and 7.....	19
Viscoelastic Properties of the Bridge.....	23
FAILURE MECHANISMS.....	25
Crushing of Vertical Web Stiffener.....	27
Cracks in Adhesive Joints.....	29
Polymer Concrete Wearing Course.....	34
Acoustic Emission Results and Interpretations.....	35
ULTIMATE STATIC LOAD TEST.....	47
Structural Failures.....	47
Deflection Measurements.....	48
Strain Measurements.....	48
Acoustic Emission Measurements.....	52
ANALYTICAL STUDIES AND RESULTS.....	54
Comparisons of Deflections.....	54
Comparisons of Strains and Stresses.....	56
SUMMARY OF FINDINGS.....	60
CONCLUSIONS AND RECOMMENDATIONS.....	61
REFERENCES.....	63



## LIST OF FIGURES

- Figure 1 Load arrangement and results of static test for transverse load distribution.
- Figure 2 Location of loading rams and steel spreader beams on test structure. Plan view of bridge deck shown.
- Figure 3 Overview of the structural testing laboratory with a cyclic load test in progress.
- Figure 4 Oblique view of steel spreader beams and hydraulic rams arranged on the bridge for cyclic load series 1.
- Figure 5 Arrangement of electronic monitoring equipment during a cyclic load test.
- Figure 6 Layout of bonded electrical resistance strain gages and mechanical dial indicators on the bridge.
- Figure 7 Deflection history of middle girder at static reference loads of 2,800 lb for load series 1.
- Figure 8 Deflection of middle girder at static reference loads showing effects of accumulated cyclic loads.
- Figure 9 Deflection of cross section of bridge at midspan for static reference loads of 4,000 lb.
- Figure 10 Deflection relaxation curves for (a) typical polymeric composite and (b) supports and interior panels of the middle girder of the bridge.
- Figure 11 Viscoelastic recovery of bridge following removal of load for series 7.
- Figure 12 Flexural cracks in the face of a vertical web stiffener at a girder end support.
- Figure 13 Typical crack in adhesive joint between flange plate and horizontal stiffener.
- Figure 14 Location of cores drilled through the polymer concrete wearing course for tensile bond test.
- Figure 15 Tensile test fixture applying a force to a 2-in diameter core in the polymer concrete wearing course.
- Figure 16 Representative fracture surfaces on core 12 showing different types of failures.

- Figure 17 Acoustic emission data for load series 1.
- Figure 18 Representative acoustic emission rates for two load series at a load rate of 5 cpm.
- Figure 19 Typical acoustic emission rates during load series 7.
- Figure 20 Typical acoustic emission traces.
- Figure 21 Amplitude distribution of acoustic emissions from load series 7.
- Figure 22 Deflections of bridge deck at load of 9,600 lb.
- Figure 23 Deflections of the bridge deck for ultimate load test.
- Figure 24 Strains in two lower chords for ultimate load test.
- Figure 25 Comparison of experimental and analytical deflections for load series 2.

## ABSTRACT

Static and cyclic load tests were conducted on a 16-ft long bridge constructed with fiberglass materials. Approximately 1.6 million cycles of loads were applied to the deck to study the fatigue characteristics of the bridge. The location and magnitude of the loads were selected to accelerate failure of elements and joints in the structure. Upon completion of the cyclic load program, an ultimate static load of 16,640 lb was reached before the bridge failed. Experimental strains, deflections, and acoustic emissions were monitored during the load tests.

Test results indicated that cracks in the bonded joints formed and extended under cyclic loading. The strength of the bridge was not impaired with the development of the cracks, but deflections increased progressively with the growth of the cracks. Viscoelastic creep occurred to a minor extent during sustained loading.

A theoretical analysis of the behavior of the bridge was conducted by means of a finite element model. The agreement between the experimental and theoretical investigations were satisfactory. Recommendations are offered to improve the performance of the structure.



## FINAL REPORT

## FATIGUE STUDY OF A GRP PEDESTRIAN BRIDGE

by

Fred C. McCormick  
Faculty Research Scientist

## INTRODUCTION

This report is the last in a series of technical reports describing the development and performance of an experimental bridge intended to carry light loads such as pedestrian traffic. (1,2,3,4,5,6) The superstructure of the bridge was unusual in that it was constructed entirely of glass-reinforced plastic (GRP) and represented a pioneering effort in synthetic composite technology when it was designed in 1976. The superstructure was composed of three identical triangular, open-web trussed girders 16 ft long, 28 in wide (top flange), and 18 in deep. Fabrication was accomplished manually in a laboratory at the University of Virginia with approximately 6 man-hours required for the assembly of each girder. Total preparation and assembly time for the bridge, exclusive of the polymer concrete wearing surface, was estimated at 450 man-hours. For the convenience of the reader, excerpts from the referenced reports are included in Appendix A to describe in greater detail the materials and design and fabrication of the bridge superstructure.

While initially intended for use as a pedestrian bridge, the structure was removed from a field test site and used as a test specimen for a series of cyclic load tests in a laboratory. The decision to discontinue exposure and traffic tests in the field provided an opportunity to obtain fatigue data from the structure which would not have been possible otherwise.

A brief chronology of the events related to the life of the subject structure, designated TTG-WC, is as follows:

- . Fall 1976. The design of the 16-ft-long-by-7-ft-wide-bridge was completed. Fabrication was completed by January 1977.
- . January 1977 until July 1982. The superstructure remained in the fabrication laboratory awaiting shipment to a test site in a rest area of an interstate highway. The rest area was never constructed, so the superstructure was placed in outdoor storage at a facility of the Virginia Department of Highways

and Transportation. Exposure to climatic elements for the next 32 months had no apparent adverse effects upon the GRP materials..

- . March 1985. The superstructure was moved to Pen Park in Charlottesville, Virginia, and erected on precast concrete abutments which had been molded to fit the support configuration of the superstructure. A polyester concrete overlay wearing course was subsequently placed on the deck.
- . September 1985. Following static and creep load tests, the bridge was moved from Pen Park to the structural testing laboratory at the University of Virginia, where cyclic load testing was conducted.
- . August 1986. The demolished bridge was removed to a disposal area following various load tests in the laboratory.

This report covers the period from September 1985 through July 1986 and describes the nature and the results of the load tests and various monitoring procedures conducted on the bridge. An analytical study was conducted during the summer to model the behavior of the structure under load.

#### PURPOSE AND SCOPE

The purpose of the research was to observe and gain an understanding of the behavior of the experimental bridge during cyclic load applications.

The principal objectives were as follows:

1. to determine the effect of cyclic loads upon the integrity of a polymer wearing course bonded to the bridge deck;
2. to determine the effect of cyclic loads upon the behavior of the structural connections between members throughout the bridge;
3. to determine the "weak-link" in the configuration of the bridge and to assess the consequences of first failure in the materials and the structural elements; and
4. to establish design criteria based on load magnitude, cyclic frequency, displacements of elements, or other suitable parameters.

## TEST CRITERIA AND PROCEDURES

The selection criteria for the application of the cyclic loads was influenced by several conditions. First, a limited time (approximately 6 months) was available for collecting test data because of restraints on funding and the availability of student assistants. Secondly, the rate of the load application was governed by the relatively slow elastic inertial response characteristics of the bridge. Thus, it was necessary either to limit the deflection amplitude of the structure and the applied load to relatively small values in order to accumulate a large number of load cycles, or to limit the number of cycles of load if large deflections were imposed on the bridge. The application of a large number of load cycles at small amplitudes typical of actual service conditions would have provided information relative to the longevity of the bridge, but would not have identified specific weak links nor failure mechanisms in the bridge, if such mechanisms turned out not to be susceptible to a fatigue type of failure. Therefore, it was decided to use a more severe load-deflection sequence for the test program than would be expected in normal service in order to accelerate failure.

### Transverse Load Distribution

The ability of the three-girder superstructure to transfer load transversely from one girder to another through the cover plate was measured by an initial static load test and by cyclic load series numbers 6 and 7. The static load test was conducted by placing the 7 ft long steel beam in the longitudinal and transverse center of one edge girder and applying a load with a hydraulic jack located at the center of the steel beam. Dial indicators were used to measure deflections of the lower chords and deck flanges at the midspans of the three girders. The deflection measurements were made for load intervals of 200, 400, 600, and 800 lb. The arrangement for the test is shown in Figure 1.

Unlike the static load test, the arrangement for cyclic load series 7 utilized two hydraulic rams located symmetrically on a single steel spreader beam placed on the middle girder instead of on an outside girder. Therefore, the load was transferred to the exterior girders by means of shear forces in the 1/4 in thick cover plate and the polymer concrete wearing surface. Differential displacements in the flange plates of the three girders were measured by dial indicators placed at the transverse center of the middle girder and at the interior edges of the flanges of the exterior girders. The principal purpose of the series 7 test was to produce a fatigue failure mechanisms by the cyclic application of shear forces between the girders as would normally occur with vehicular wheel loads applied to a single girder on a prototype structure. Therefore, large displacements (up to 0.9 in) were used on the center girder to generate a severe testing environment to accelerate the development of an identifiable mode of failure.

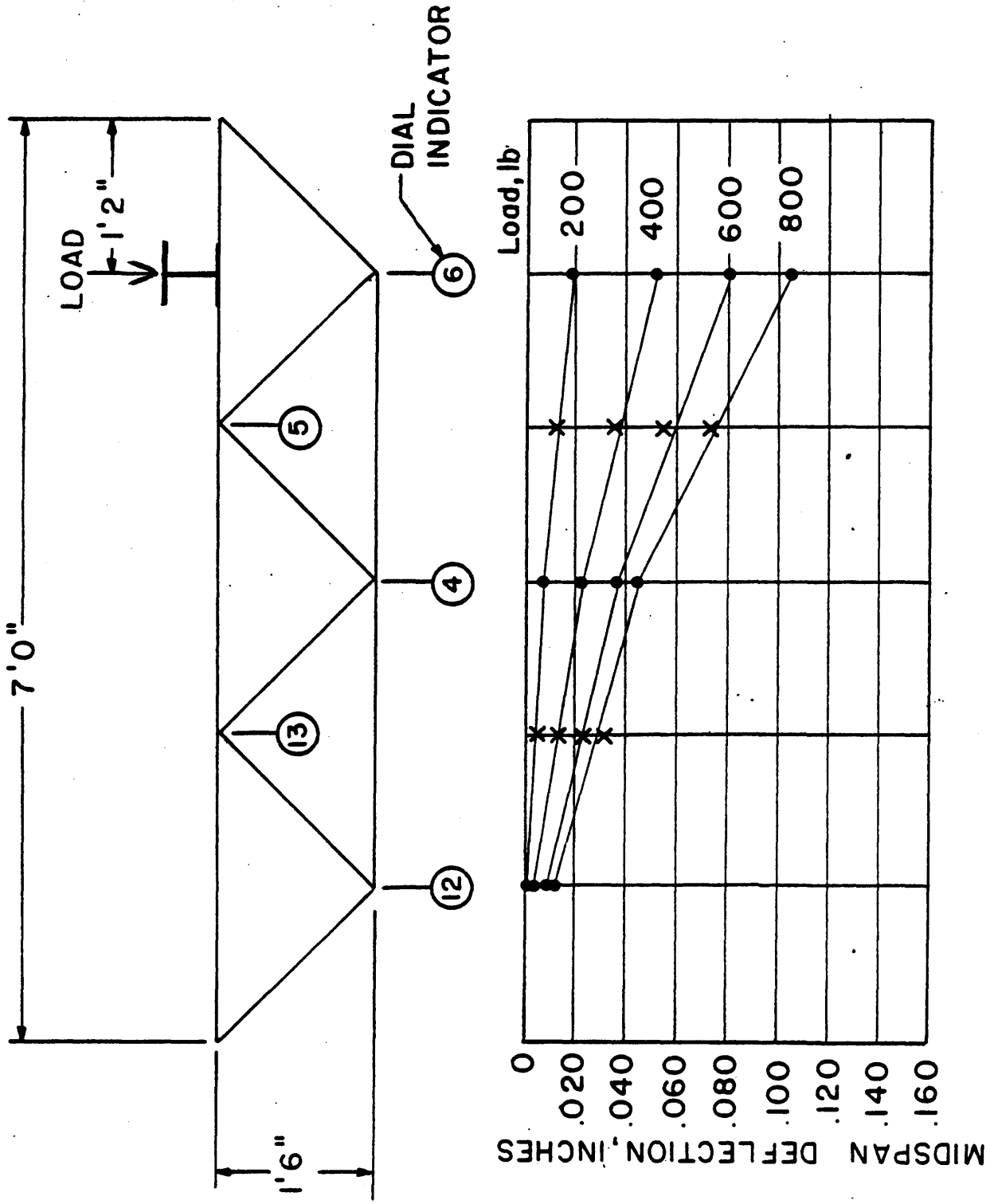


Figure 1. Load arrangement and deflections at midspan of static test for several transverse loads.

### Cyclic Load Sequences

A review of the technical literature provided no guidance for extrapolating fatigue data in a load-time domain for a GRP structure of the type under study, so reliance was placed on experience with an earlier developed girder which had been loaded to a deflection/span ratio of 1/500. That girder had failed in an adhesive joint after 407,000 cycles of load. Based on this experience and an estimate of the load cycles at the maximum design load over a period of 20 years, a value of 500,000 load cycles was selected for the first series of loads. The applied load produced a midspan deflection of 1/1,000 of the span. Subsequent load-cycle combinations are shown in Table 1. In all of the load series, an effort was made to maximize the range over which the bridge deflected in order to magnify the deformations in the structural elements and connections as much as possible. As the testing progressed, several changes in procedures and instrumentation were made to adjust to aspects of the performance of the bridge which had not been anticipated in the planning phase. These changes will be noted as they apply to the reported test results.

It was not feasible to apply a uniformly distributed load to the bridge deck, so the load was applied through steel spreader beams at various locations on the structure as shown in Figure 2. Thin sheets of plywood and neoprene were used as shims between the steel beams and the bridge surface to equalize the applied force along the length of the beam. Mechanical displacement gages mounted beneath the deck confirmed that the vertical deflections were uniform across the width of the bridge. Loads were applied to the steel beams by means of hydraulic rams controlled by a Reihle/Los fatigue testing machine. The rate of loading selected for the different load series ranged from 5 to 15 cycles per minute, depending upon the magnitude of the load-deflection ranges of the load series. It is not believed that the differences in the load rates affected the structural performance of the bridge in any way.

Figure 3 is an overview of the testing laboratory with a load test in progress. Figure 4 is an oblique view of the spreader beams and rams as arranged for load series number 1.

### Ultimate Static Load

Upon completion of all cyclic load series, a static load was applied to the bridge until the positive failure of a member occurred. The magnitude of this load was considered the ultimate load for the entire structure. The load was applied with the same arrangement as that used for load series 7.

TABLE 1  
Series of Cyclic Load Applications

Series	Date Started	Static Test Load, lb	Cyclic Load Range, lb	Load Arrangement, per Fig. 1	Reference Dial Gage	Number of Rams	Deflection Range, in	Total Load Cycles	Rate of Load cpm
1	12/12/85	2,800	1,200-3,000	(a)	#4	2	0.10-0.23	500,000	13
2	2/19/86	2,900	1,200-2,900	(b)	#2	1	.10- .28	250,000	13
3	3/05/86	4,000	1,600-4,000	(b)	#7R	1	.25- .50	150,000	9
4	3/21/86	2,000	3,200-5,600	(b)	#7R	1	.45- .66	158,000	12
5	4/08/86	2,000	2,200-5,600	(b)	#7R	1	.57- .90	18,000	5
6	4/17/86	4,000	2,400-6,400	(c)	#4	2	.25- .50	75,000	5
7	5/02/86	4,000	6,400-8,800	(c)	#4	2	0.60-0.90	468,000	10

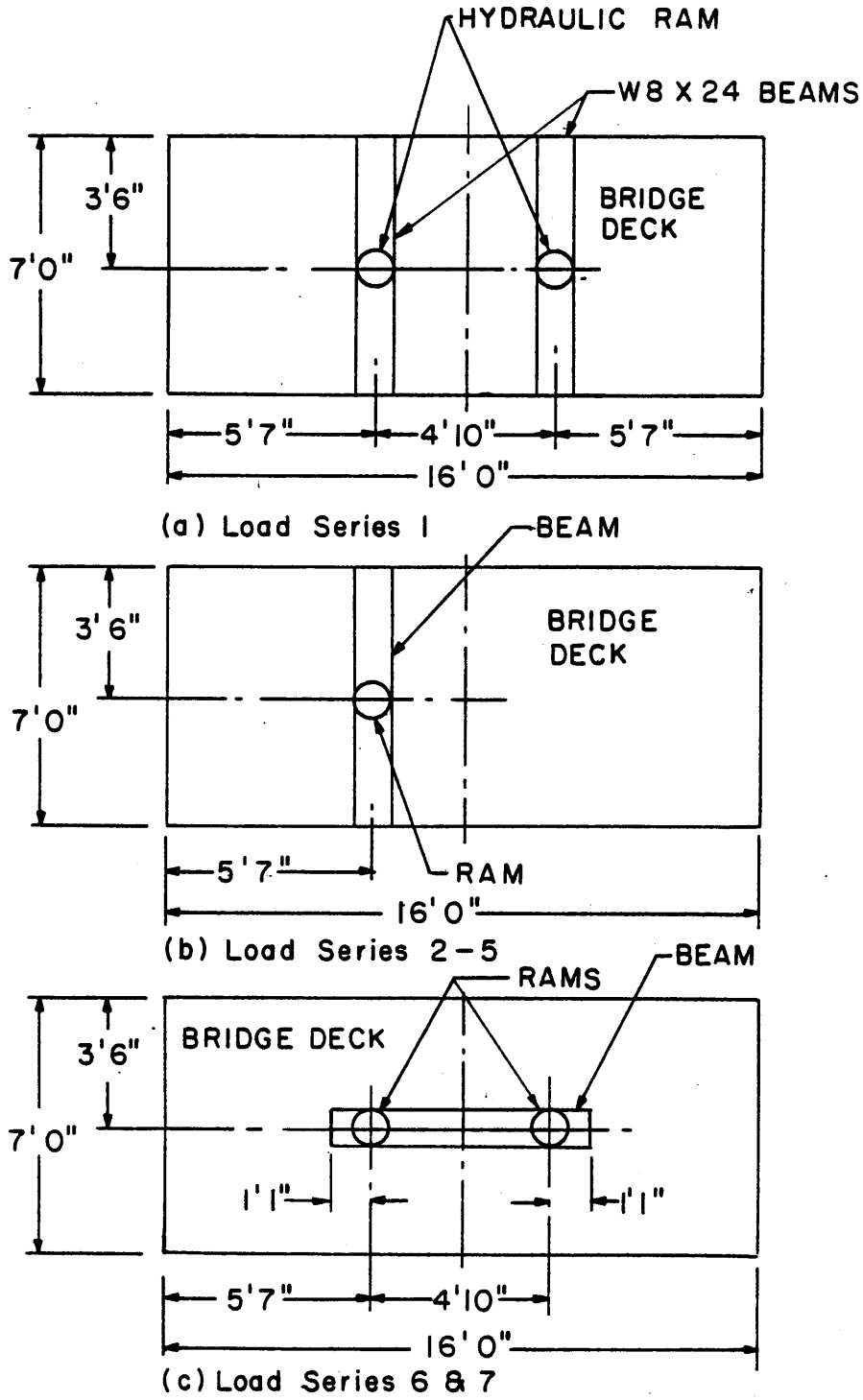


Figure 2. Location of loading rams and steel spreader beams on test structure. Plan view of bridge deck shown.

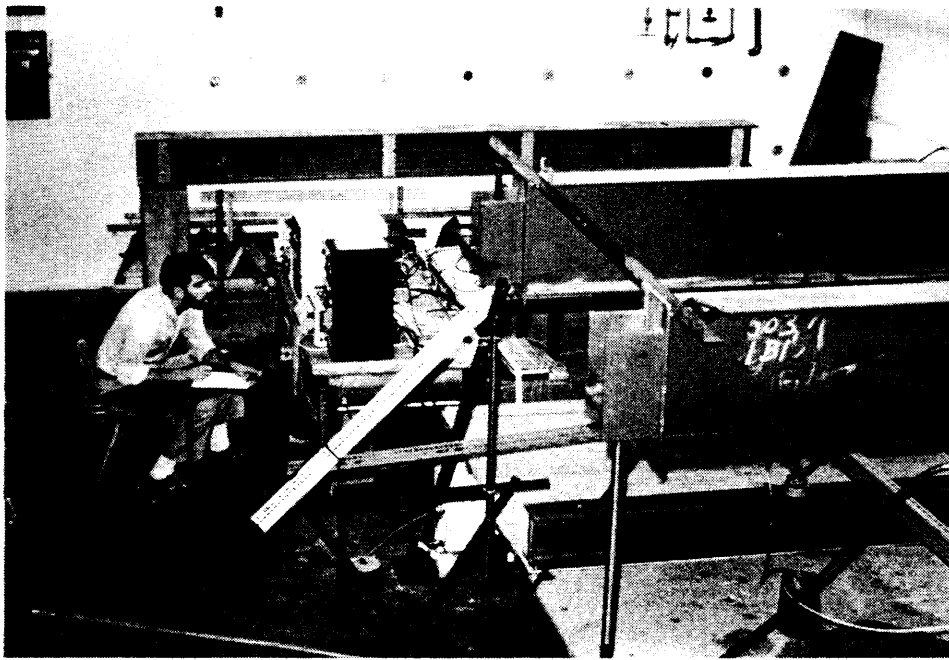


Figure 3. Overview of the structural testing laboratory with a cyclic load test in progress.

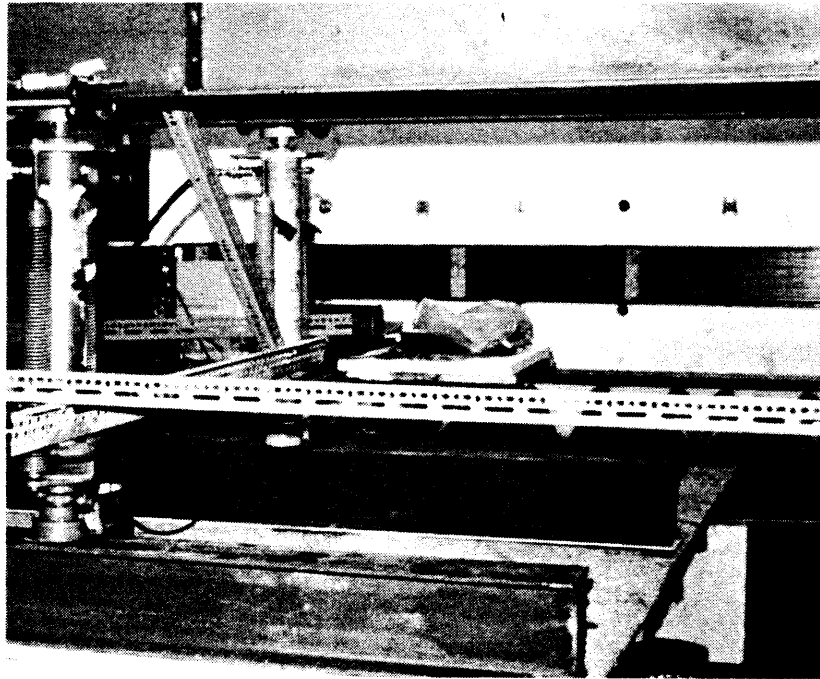


Figure 4. Oblique view of steel spreader beams and hydraulic rams arranged on the bridge for cyclic load series 1.

### Monitoring Instrumentation

Three systems of monitoring instruments were used to observe the behavior of the bridge during the load tests: electrical resistance strain gages, mechanical dial indicators, and acoustic emission equipment. Figure 5 is a view of some of the electronic indicating and recording instrumentation.

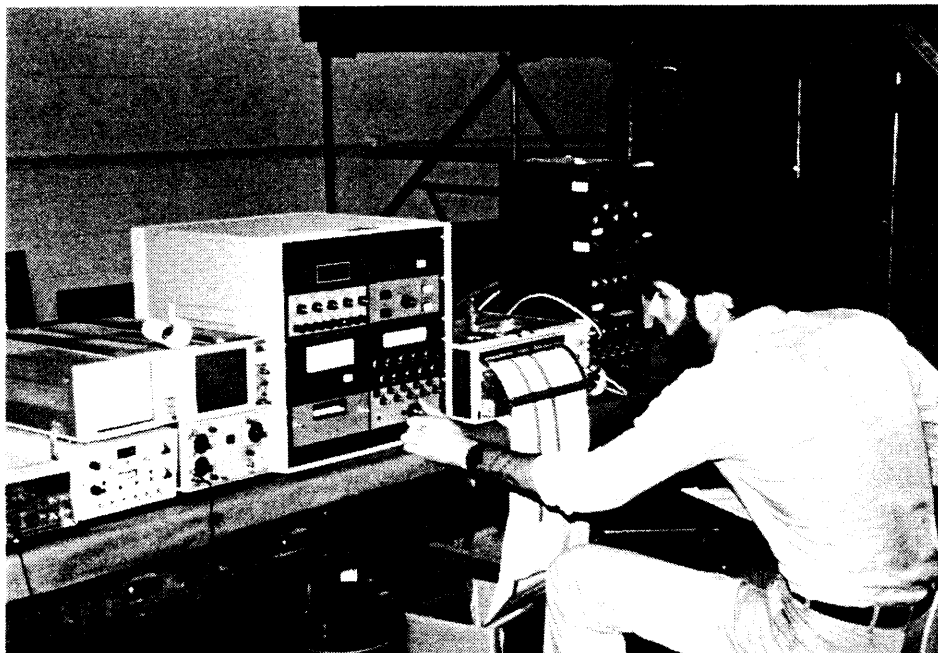


Figure 5. Arrangement of electronic monitoring equipment during a cyclic load test.

- Electrical resistance strain gages -- A total of 23 strain gages were bonded to various elements of the girders. A layout of the gages is shown in Figure 6. The gages and adhesives were supplied by Micromeritics, Inc. They were either EA-06-250BF-350 or EA-06-500BL-350 foil gages and the bonding adhesives was AE-10 epoxy, which was cured at room temperature. Voltage measurements for the gages were made with strain indicators, Model V/E-20, and channel switching equipment furnished by Micromeritics, Inc.
- Dial indicators -- A total of 18 mechanical indicators were used to measure vertical displacements of various points of the three girders. The layout of the gages is also shown in Figure 6. Various standard makes of gages -- Ames, Tumico, etc. -- were used as they were available in the laboratory. All gages were readable to the nearest 0.001 in and were visually accessible throughout the testing period.
- Acoustic emission equipment\* -- Two acoustic emission (AE) signal processors, Models 203 and 204B, were used in conjunction with a Model AC175L (175 kHz frequency) sensor mounted on the bridge. All acoustic emission equipment was furnished by Acoustic Emission Technology, Inc. Many of the AE data were recorded with a signal amplification of 88 dB in order to match the count rate of the two processors. Efforts were made to eliminate background (loading equipment) noise by selecting an appropriate signal threshold value (1.31 volts for the Model 204B unit) and insulating load and support points with elastomeric pads to minimize the transmission of external mechanical vibrations. In spite of these efforts, it appears that most of the emissions recorded resulted from the rubbing action of contact surfaces within the bridge or from external contact at the supports and load points. Periodic photographs were made of the amplitude distribution image of the emissions as displayed by the Model 203 unit to assist in determining the source of the emissions.

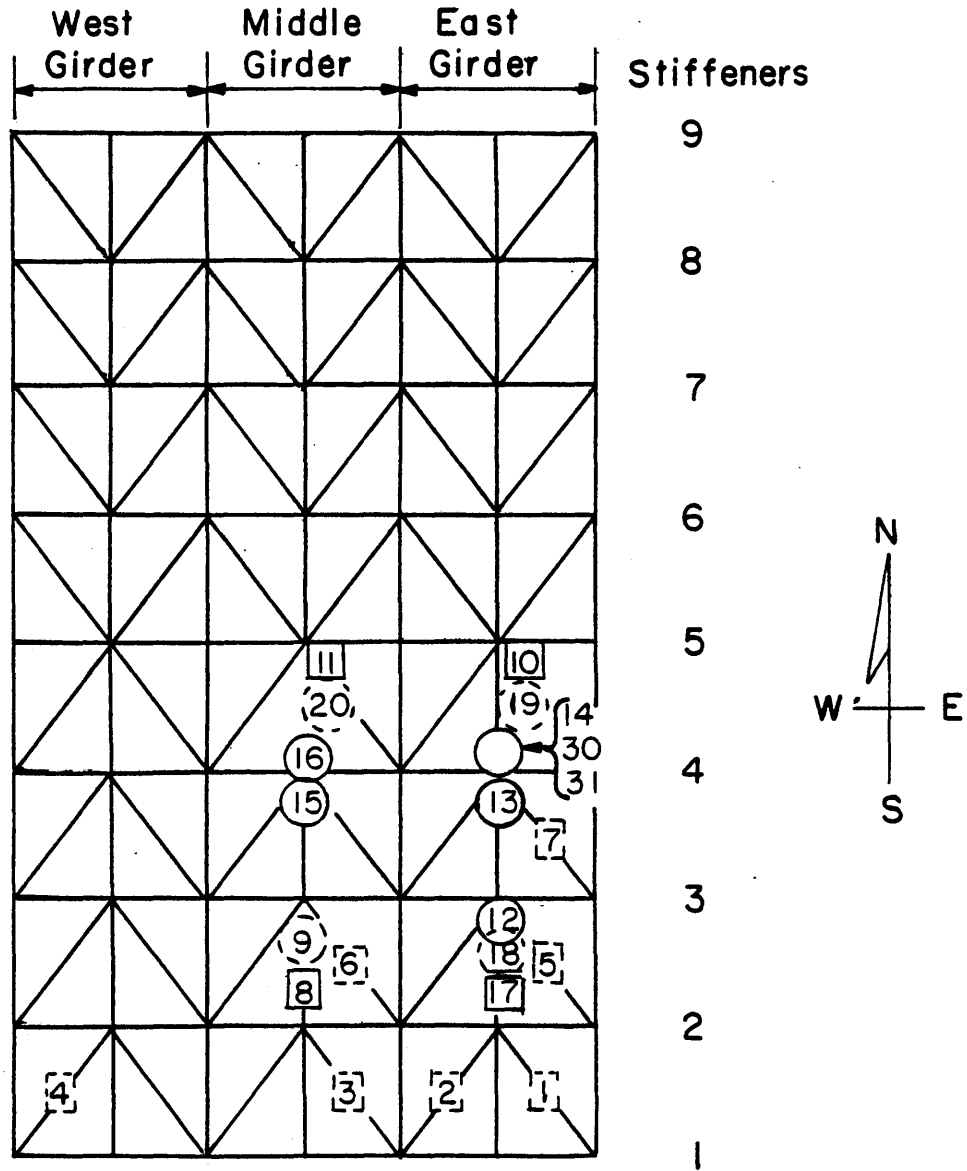
## TEST RESULTS

### Transverse Load Distribution

The transverse distribution of a load from one girder to another was proportional to the deflection of the several girders, as long as the members remained elastic and did not buckle. Figure 4(b) shows the

---

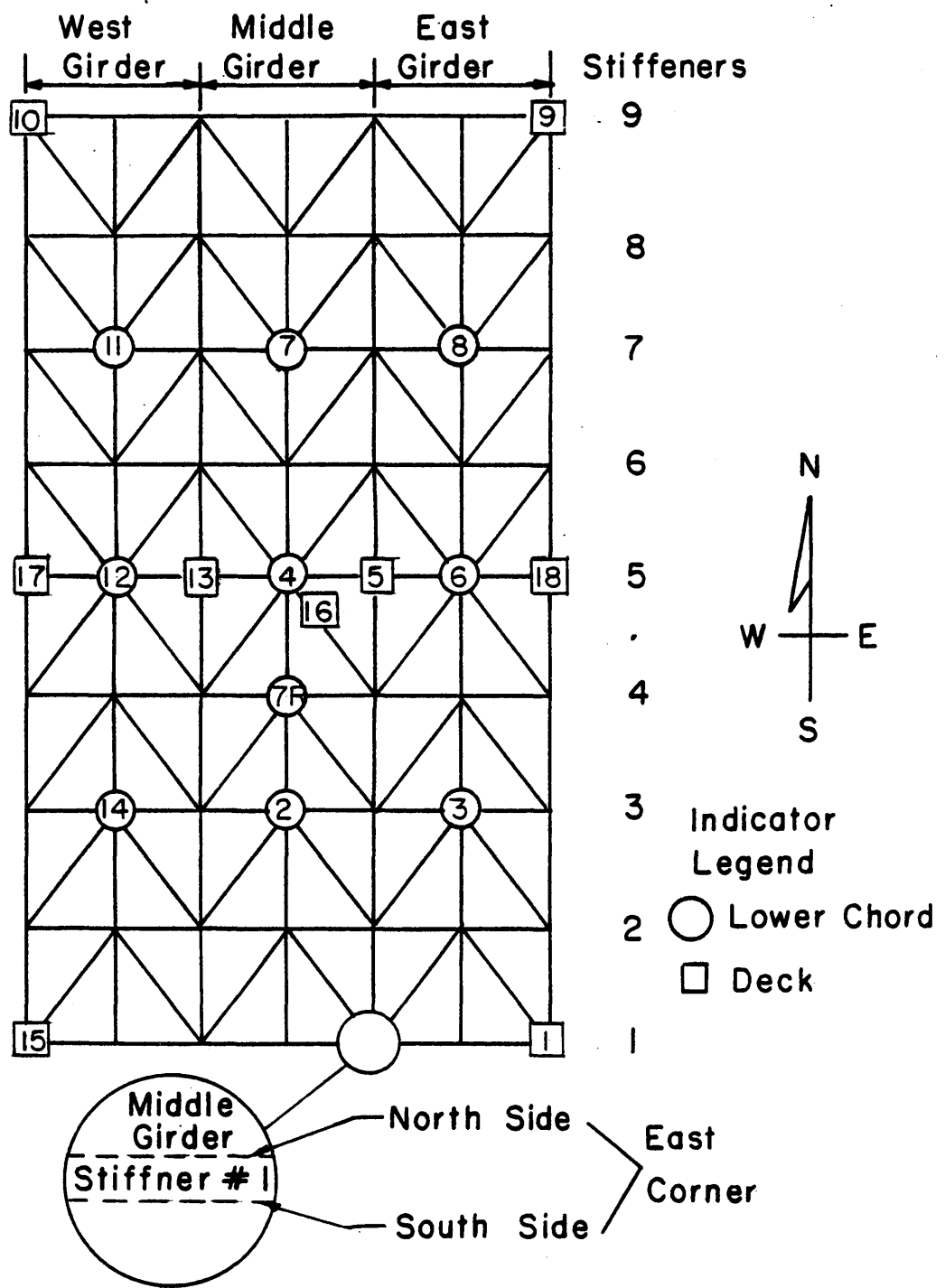
\* For terms relating to acoustic emission technology, see ASTM Standard E610-77, "Standard Definitions of Terms Relating to Acoustic Emission," American Society for Testing and Materials.



**Legend**

- [ ] Diagonal Web Elements
- [ ] Top of Plate
- Lower Chord
- Bottom Plate

Figure 6(a). Layout of bonded electrical resistance strain gages and mechanical dial indicators on the bridge.



**Key to Table 3 Nomenclature**

Figure 6(b). Location of deflection indicators and key to Table 3 on plan view of the bridge.

vertical displacements which occurred along the cross section at the midspan of the bridge with the application of the test loads. The lines connecting the data points in the figure indicate that the deflection ratios between girders increased slightly with an increase in the load on the outside girder. For example, at the 600- and 800-lb loads, the lower chord deflection ratios between the loaded and adjacent middle girder was 2.1 and 2.3, and for the exterior loaded to exterior unloaded girder was 10.0 and 10.6, respectively. When superimposed on the plotted shape of the lower chord deflections, the measured deflections of the deck plate indicated that the entire superstructure was acting as a unit without differential displacements between the girder flanges and lower chords. While no determination was made in this test of the torsional distortion of the girders along their longitudinal axes, it is obvious from the displacement of Figure 4(b) that torsional stresses would be induced with eccentric load applications to the bridge.

The effect of lateral load transfer and torsional measurements will be considered further when the behavior of the bridge under nonsymmetrical cyclic loading is discussed.

#### Cyclic Load Tests

It was presumed at the outset that the condition of the bridge prior to a given test would not adversely influence the findings from the test. This presumption obviously was inaccurate in an exact sense, and it is not known to what degree the damage from one test sequence affected the behavior of the structure in a subsequent test, but each test series was "zeroed" at the beginning with existing damage being recorded as reference for comparison. Thus, the incremental damage inflicted during each test procedure could be attributed to the performance of the specific test. While it would be improper to apply this logic under an assessment of the behavior of a virgin structure under a given test on an absolute scale, the consideration of the behavior on a relative scale -- one type of test versus another type of test -- may indicate an accumulation of damage and the overall behavior of the bridge in resisting the effects of cyclic loads. The answer to the question, Does the bridge fatigue easily? remains as the focal point at issue, whatever the means of addressing the point.

It should be recalled that the true condition of the bridge when installed in the testing laboratory was unknown, except that several members obviously had been damaged and subsequently repaired during the four times the bridge was loaded and unloaded from a lowboy carrier. The presence or initiation of small cracks could not be determined. Also, it should be remembered that the bridge had been loaded previously with a uniformly distributed load of 8,000 lb, of which 6,000 lb were sustained for two months when ambient temperatures ranged from 40°F to over 90°F. A visual damage survey prior to laboratory testing revealed the following information.

1. The outside vertical stiffeners at the supports of the center girder were broken at the lower connector. This damage was effectively repaired with plates bonded to the stiffeners.
2. Several of the interior support stiffeners in the outside girders were cracked at the lower connectors. These were not repaired since the cracks did not appear to be in a stressed region of the element.
3. A crack between the horizontal stiffener and the flange was observed at one end of the center girder.
4. None of the internal stiffeners nor connectors appeared to be misaligned nor damaged in any way other than for surface abrasion.
5. The polymer concrete wearing surface appeared to be intact over the deck area.

Cyclic loads were applied to the deck through steel spreader beams as shown in Figure 2(a). Load series 1 was conducted with loads applied symmetrically and distributed transversely about the midspan, whereas load series 2 through 5 were applied nonsymmetrically. All three girders were loaded equally in these load series. Load series 6 and 7 were applied symmetrically about the longitudinal center of the middle girder only and distributed longitudinally by means of one spreader beam. Therefore, the exterior girders were loaded indirectly and eccentrically in series 6 and 7 by the shear forces transmitted through the deck structure from the middle girder.

#### Load Series 1

In the first load series, 500,000 repetitive loads were applied at a rate of 13 cycles per minute. The load range was held constant with a minimum of 1,200 lb and a maximum of 3,000 lb each cycle. The deflection of the lower chord of the middle girder at the midspan of the bridge (reference gage #4; see Table 1 and Figure 6) ranged correspondingly from 0.10 to 0.23 in for each cycle. With the completion of a selected number of load cycles, usually 50,000, the cyclic loading was interrupted long enough to conduct a static load to assess the damage to the structure due to the preceding increment of load applications. All deflection gage and strain gage readings were recorded and acoustic emission activity was monitored for any counts emitted during the period the static load was held. However, no emissions were noted during any of the hold periods of any of the load series, except number 7. The reference load for the static test for series 1 was 2,800 lb. The reference loads for the other load series are shown in Table 1.

Figure 7 presents the results from the 11 static load tests for load series 1 plotted for a longitudinal section of the bridge at midspan. The data are plotted without correction for displacements or settlements at the supports, the values for which are shown plotted in Figure 7 as well. These data are representative and typical of the deflection data at other sections through the structure. It is clear from the sectional profiles that the deflection of the bridge increased progressively throughout the cyclic load testing.

Figure 8 presents the same deflection values as in Figure 7 in a slightly different way to show the rate of increased deflection with time or the number of cyclic loads. Data from load series 2 and 7 are also included in the figure. Normalized deflections were computed by subtracting the value of the deflection at the reference static load prior to the cyclic load series from each of the deflections measured at subsequent static loads applied within the given load series. Scatter in the plotted values occurred due to slight variations in the reference load readings and creep of the structure at the time the deflection measurements were recorded. Errors in reading the static load indicator were approximately 0.004 of the nominal value. The data from the different load series in Figure 8 cannot be compared directly since either the reference static load values, the load arrangements, or the reference dial indicator were different in the several cases. It should also be remembered that the performance of the bridge in each chronologically succeeding load series was dependent upon the condition and state of damage inflicted upon the structure by all preceding load cycles. With this in mind, the data from series 7 can be seen to indicate that the strength of the bridge was adequate to transfer applied loads from one girder to another through the deck assembly, and that no cataclysmic load failures occurred which modified the behavior of the structure from any of the previous cyclic load applications. It is significant that the characteristic bilinear form of the plotted data (curves A, B, and C of Figure 8) indicates that once a loading pattern was established for the bridge, deflections at a prescribed static load increased progressively at a constant rate (within the scatter band) with increasing numbers of load cycles. Curve D is shown as an alternate interpretation of the data for load series 7 wherein the results suggest that the rate of damage to the structure increased significantly after approximately 350,000 cycles of load. In any respect, the establishment of the rate of deflection vs load cycles would provide an extrapolated estimate of the long-term fatigue effect of cyclic loads upon the deflection of the bridge.

Linear curves were fitted to the data beyond the shakedown knee by means of least-squares computations as follows:

<u>Curve</u>	<u>Relation</u>
A	$y = + .0102 + (3.2 \times 10^{-8})x$

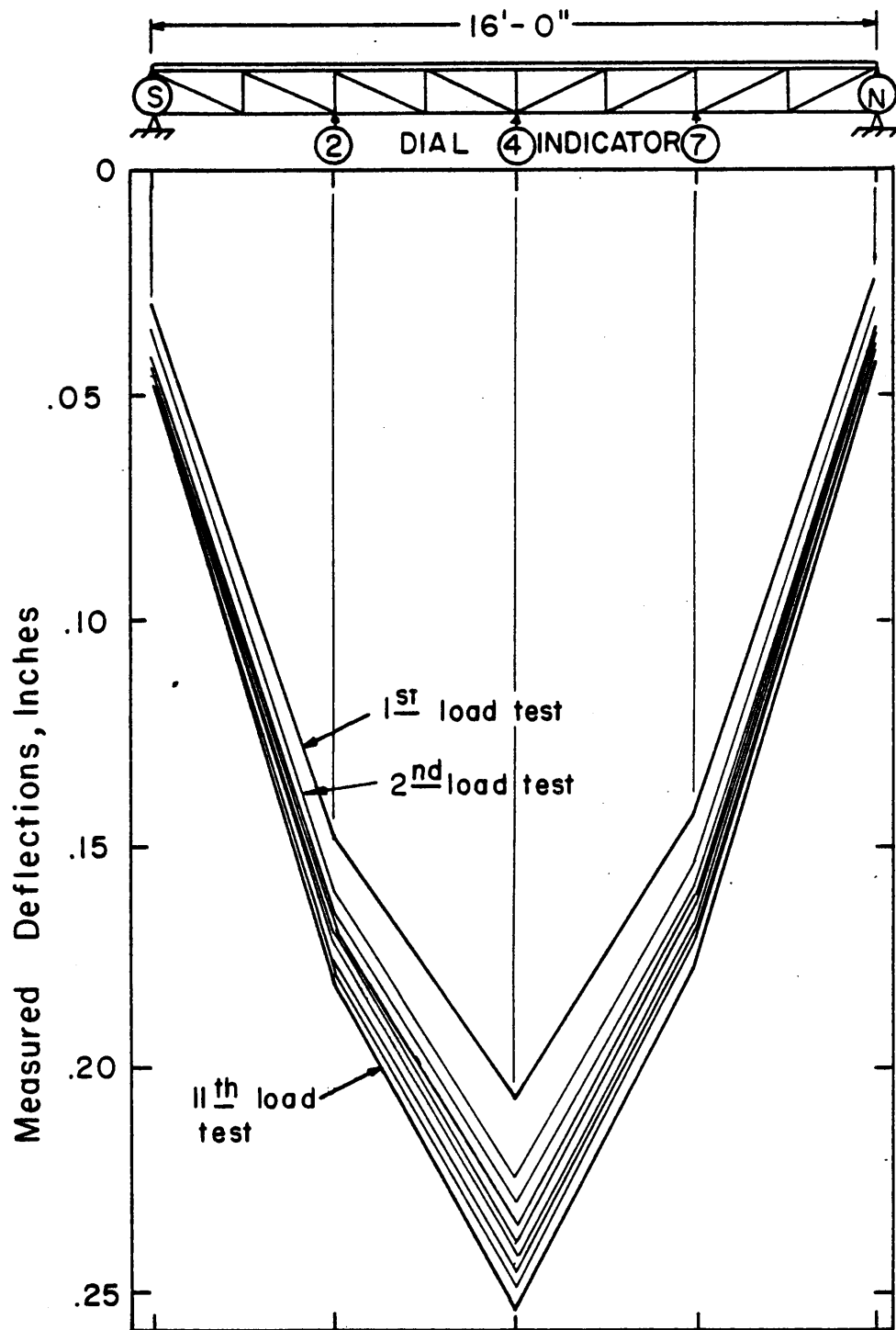


Figure 7. Deflection history of middle girder at static reference loads of 2,800 lb for load series 1.

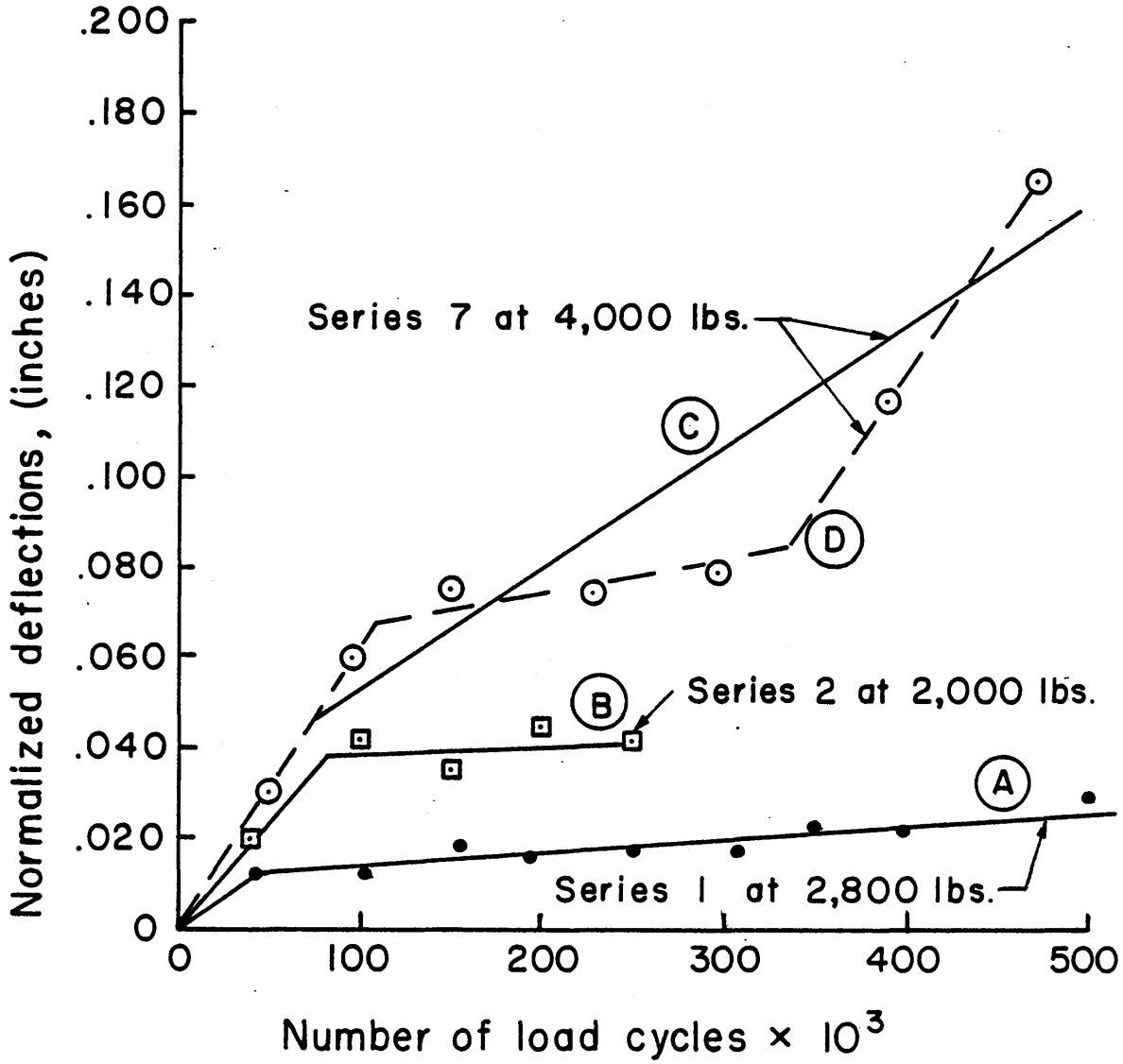


Figure 8. Deflection of middle girder at static reference loads showing effects of accumulated cyclic loads.

$$\begin{aligned}
 \text{B} \quad & y = + .0371 + (1.8 \times 10^{-8})x \\
 \text{C} \quad & y = + .0254 + (2.57 \times 10^{-7})x \\
 \text{D} \quad & y = + .0556 + (8.3 \times 10^{-8})x, \text{ and} \\
 & y = - .0658 + (4.9 \times 10^{-7})x
 \end{aligned}$$

where

$y$  is normalized deflection in inches, and

$x$  is the number of cycles of load.

Using the relation for load series 1 with  $x$  equal to 2 million cycles, a deflection of 0.74 in at the midspan of the bridge would be expected. The "normalized" deflections used in Figure 8 were not adjusted for either the elastic rebound or the viscoelastic recovery of the structure after the load was removed. The total displacements remaining in the bridge after the removal of live load were, therefore, dependent upon the length of the time following load removal as well as the elastic characteristics of the structure. The viscoelastic recovery characteristics of the structure are discussed in a section following the load series.

#### Load Series 2 through 5

With the discovery of an incipient crushing failure in one of the vertical stiffeners at a support during load series 1, it was decided to protect the stiffener by shifting a disproportionate amount of the applied load to the opposite end of the girder through a single ram located as shown in Figure 2(b). The protective measures worked nicely because the crack pattern in the stiffener remained stable throughout load series 2 through 5. The diagonal web members in the girder panels adjacent to the load beam (see Figure 1) remained grossly buckled throughout the nonsymmetrical load tests. The shear in the panel, 2,250-lb maximum for series 4 and 5, was therefore transmitted essentially by the deck assembly. As shown in Table 1, the magnitude of the maximum load was increased from 2,900 lb for series 2 to 4,000 lb for series 3 and then to 5,600 lb for series 4. The magnitudes of the lower loads were governed by the deflection amplitudes and the desired rate of loading. The principal difference between series 4 and 5 was the increased range of the deflection amplitude in series 5, which was adjusted by varying the load rate and the load range. Since the cyclic deflection range of the bridge had virtually stabilized at 0.20 in at the end of series 4, load series 5 was conducted to explore the effect of an increased range (0.33 in) of cyclic deflections upon the fatigue resistance of the structure. When it became apparent that the selected parameters were not producing accelerated failure of the joints, load series 5 was terminated.

Load series 2 and 3 proceeded through the number of planned cycles (250,000 and 150,000, respectively) without incident. Deflection and strain data from the static reference loads were obtained without difficulty and appeared consistent with expected results. However, when the load was increased for series 4 from series 3, it became evident that the high flexural compressive stresses and vertical shear deformations in the deck assembly caused a progressive upward buckling of the deck. The deflected shape was quite visible to the eye and became more pronounced as the number of cycles of loads increased. Even though the deck assembly did not appear to be in danger of buckling elastically into a collapse mechanism, the viscoelastic growth of the deflection was sufficient to lift the vertical stiffeners in the midspan panel away from their connectors at the lower chords. Removal of the applied load failed to restore the deck to an undeformed condition. For this reason, it was necessary to revert to the load arrangement of series 1 with two symmetrically positioned rams to eliminate buckling of the deck when obtaining the static reference load data.

#### Load Series 6 and 7

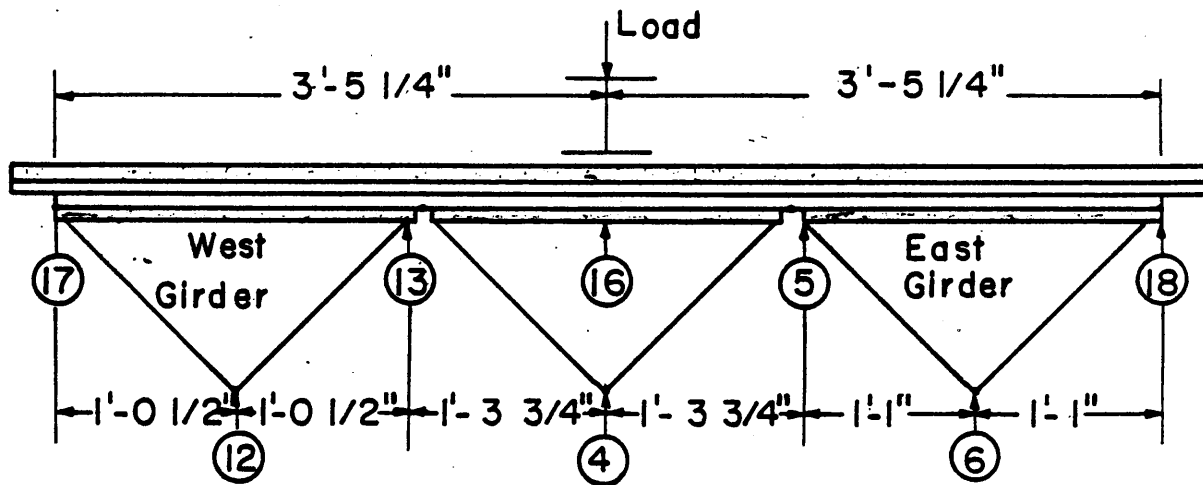
As described previously, steel spreader beams were used to transfer the applied loads laterally and equally across the three girders in load series 1 through 5. Since the bridge appeared to be undamaged (except for one support element) from the previous 1,076,000 cycles of load, it was decided to investigate the ability of the deck assembly to transfer cyclic loads laterally from one girder to another. The use of two rams located on the middle girder as shown in Figure 2(c) was selected for this test configuration. It was realized that the increased reactive force on the damaged stiffener at the support could cause a crushing collapse of that member, but at the same time it would provide information about the ability of the structure to redistribute internal forces from one overstressed element to another less-stressed companion.

The parameters of load series 6 were selected with a limited number of cycles to principally observe the behavior of the deck wearing surface and cover plate over the longitudinal joints between the girders. It was anticipated that in time and with sufficiently high shear loads transferred across the joints, cracks would appear in the polymer concrete wearing course in the regions of maximum flexure. However, at the end of 75,000 cycles of load, no signs of distress had appeared in the wearing surface and only a small amount of crack growth had been detected in the damaged support stiffener. Therefore, load series 6 was terminated and series 7 was initiated with an increase in the mean cyclic load of 73% in an effort to accelerate a failure mode in the bridge. With the application of a maximum cyclic load of 8,800 lb, the previous maximum static test load of 8,000 lb was exceeded for the first time. Corresponding initial midspan dynamic deflections at the beginning of the load series ranged from approximately 0.65 in to 0.80 in when the load rate was 10 cycle/min and the load range was from 6,400 lb to 8,800 lb. As a result of either creep of the various joints and

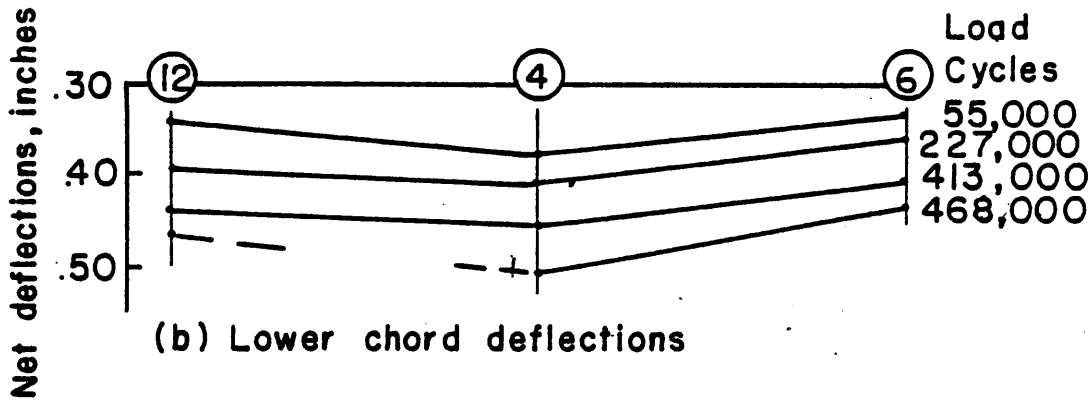
elements throughout the bridge or of slight movement of the elements with the propagation of cracks in the joints, the range of the dynamic deflections increased gradually throughout the load series. For example, the deflection range was 0.80 to 0.95 in after 270,000 cycles of load compared with the initial 0.65 to 0.80 in at zero cycles. As with the other load series, a measure of progressive damage during load series 7 was evidenced by the increase in the deflections observed at the periodic static reference loads of 4,000 lb. The data for series 7 are plotted in Figure 8.

Further consideration was given to the localized failures, displacements, and rotations of the deck assembly at the midspan of the bridge. Additional deflection indicators were installed to measure differential displacements of the girder flanges as shown in Figure 9(a). Table 2 presents static load-deflection data and calculated rigid-body rotations of the outside girders for the cross section at the midspan after 279,000 cycles of load. The test results in Table 2 indicate that the rotations of the east girder were larger than those of the west girder. This was probably due to the damaged support stiffener at the north end of the west girder, which "softened" the torsional resistance of the member. The load-rotation data appear quite linear for both girders after the first load increment. The linearity indicates that there were no significant failures in the deck assembly at the time of the test. These differential angular rotations of the segments of the deck are small, and while repetitive "dishing" of the deck could be observed visually during the cyclic load applications, the twisting of the deck elements apparently was not large enough to cause detectable failure at the level of loads applied. Further reference to this mode of distortion will be made later in the section on failure mechanisms.

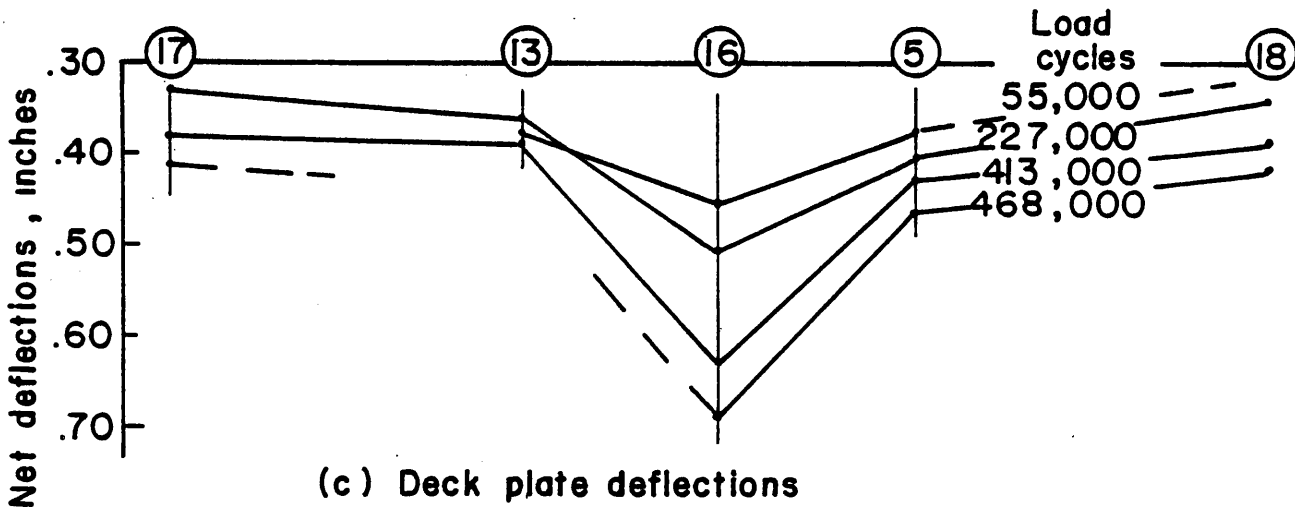
The deflection results presented in Figure 9 for several static reference loads at 4,000 lb emphasize the progressive damage effects of the cyclic loads and the differences in the deflections of the deck of the bridge and the lower chords of the girders. The deflection measurements were made immediately following the indicated number of load cycles to minimize the effect of relaxation upon the value of the deflection readings. Experience had shown that considerable variation occurred in the values of the static load deflection readings if the bridge were permitted to "rest" with the test load removed. The load arrangement of series 7 produced localized bending of the deck of the middle girder in a transverse direction, in addition to bending of the entire bridge in the longitudinal direction. The readings of dial indicator 16 reflected both of these displacements, as is evident from the relatively large deflection for that gage in Figure 9(c). The differences in the deflections of gages 16 and 4 were approximate measures of the transverse bending of the deck of the middle girder alone, if the deformations in the vertical stiffeners connecting the flange to the lower chord are neglected. As seen from Figures 9(b) and



(a) Location of deflection gages



(b) Lower chord deflections



(c) Deck plate deflections

Figure 9. Deflection of cross sections of bridge at midspan for static reference loads of 4,000 lb.

TABLE 2

Static Load and Elastic Deflection Data for Outside Girders after 279,000 Cycles  
of Load in Series 7

Load, lb.	Deflection Indicators (See Figure 9(a))							Flange Rotation	
	12, in	13, in	17, in	6, in	5, in	18, in	West Girder, Degrees	East Girder, Degrees	
0	.000	.000	.000	.000	.000	.000			
1,600	.130	.142	.124	.124	.141	.108	.041	.073	
3,200	.255	.275	.247	.248	.268	.220	.064	.106	
4,000	.320	.338	.305	.305	.330	.272	.076	.128	
4,800	.380	.405	.366	.367	.394	.330	.089	.141	
6,400	.498	.532	.481	.483	.517	.432	.117	.187	
8,000	.615	.655	.595	.596	.635	.540	.138	.209	
8,800	.679	.720	.653	.653	.698	.595	.154	.227	

9(c) the transverse bending of the deck ranged from .084 in to .092 in after completion of 55,000 cycles and 227,000 cycles of load, respectfully. respectively. The increase in the relative displacements as indicated by gages 16 and 4 was due to either creep in the deck materials, delaminations at the interfaces in the deck assembly or a combination of both. Visual inspection of the polymer concrete wearing surface at intervals throughout the tests did not reveal any cracking, spalling, or crushing of the concrete surface. Minor cracking or interfacial bond failure made have occurred without detection.

### Viscoelastic Properties of the Bridge

Viscoelastic behavior was clearly demonstrated by the bridge with the removal of a load that had been sustained for sometime. A positive load was sustained over a number of days since the lower bound of the cyclic load range was always greater than zero. The interruptions of the cyclic loads to conduct periodic static reference load tests usually were approximately 15 minutes in duration and therefore didn't provide sufficient time for the bridge to rebound or recover appreciably from the sustained load. Several measurements were made, however, of the rebound deflections of the structure in an effort to ascertain the residual displacements in the structure due to damage of joints and members.

Ordinarily, one would expect a relaxation curve for a glass-reinforced polymeric composite to follow a form similar to the one shown in Figure 10(a). Following the 150,000 cyclic static load test of series 1, relaxation deflections and strains were recorded for a period of 81 hours. The deflection data from this investigation are shown in Figure 10(b) for the middle girder. Data from the two outside girders were quite similar. It is observed that the general shape of the relaxation curves for the supports (indicated by gages 9-10 and 11-15) corresponds to that of the typical polymeric composite. It is believed that the shape of the support curves was generated principally by the action of the elastomeric bearing pads and overall recovery of the bridge. However, the shapes of the curves defined by gages 2, 4 and 7 contain an irregular "hump" which may be attributed to viscoelastic buckling of the deck assembly during the period of sustained load. When loaded, the buckled shape of the deck (upward displacements between the load points) was so minor that it was undetectable by eye or by the instruments when compared with the relatively large downward displacements of the deck. With the removal of the live load, the elastic upward rebound of the bridge resulted in a residual deflection (0.35 in at gage 4) which diminished further with time. Simultaneous with the continuing viscoelastic recovery of the bridge as a whole, the deck began to recover viscoelastically from its upward buckled shape to its normally straight shape, which produced a net downward movement of the

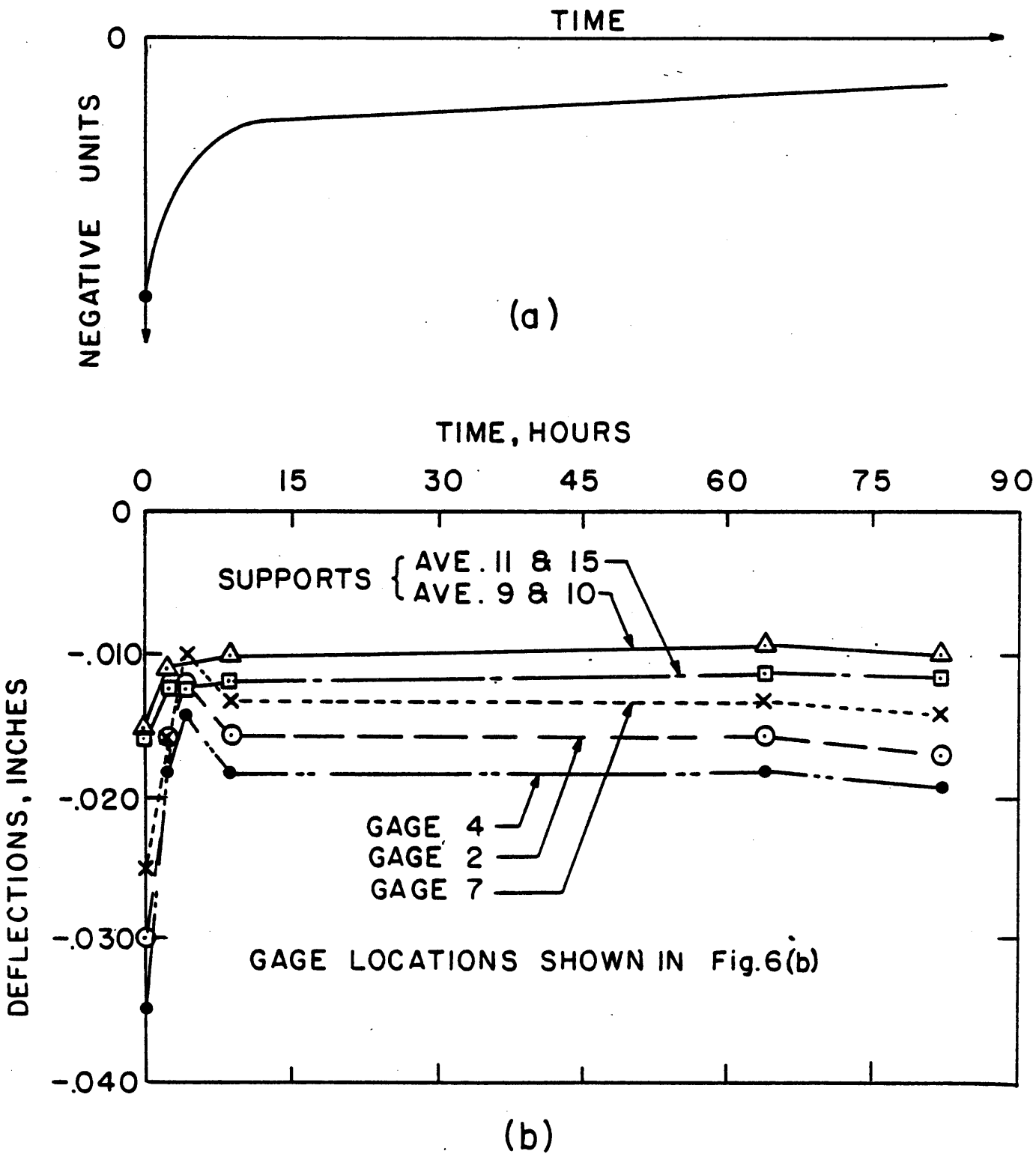


Figure 10. Deflection relaxation curves for (a) typical polymeric composite and (b) supports and interior panels of the middle girder of the bridge.

center portion of the structure. After approximately 4 hours, the rate of the downward movement of the deck exceeded the rate of the upward movement of the overall bridge and formed the "hump" in the deflection curves shown. Several bonded strain gages monitored with a continuously plotted record over the relaxation period disclosed similar "humps" in the recovery data.

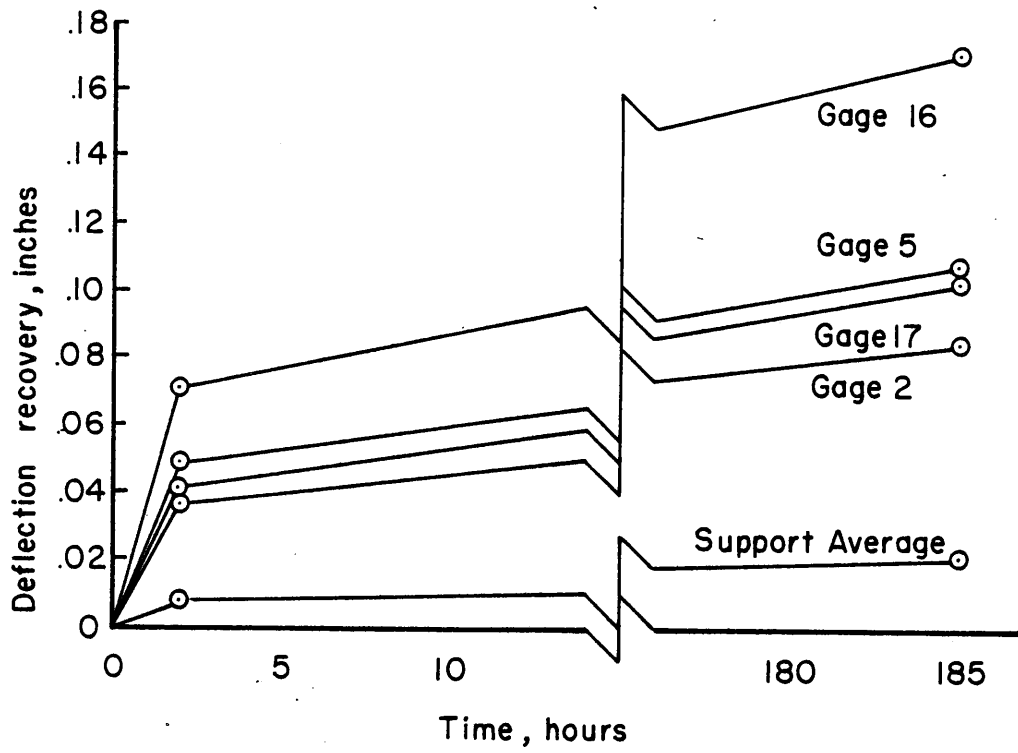
The buckled shape of the deck, while imperceptible in the symmetrical load arrangement of series 1, was obvious in series 4 and 5. In fact, the buckled deformation on the deck became so pronounced at the loads applied in series 4 and 5 that the dial indicators were unstable during the static reference load test and no valid deflection data could be obtained with the unsymmetrical load arrangement. Therefore, the static reference loads for series 4 and 5 were applied through two rams in the symmetrical arrangement described for series 1. This procedure (using a static load value of 2,000 lb) provided stable and comparable deflection data.

Upon completion of load series 7 and the removal of all loads, the deflection recovery of the bridge was observed. Figure 11(a) presents comparative data for several representative deflection indicators wherein readings were taken at 2 and 184 hours after removal of the test load. Gages 16 and 5 and the support gages were in contact with the deck and gage 2 was in contact with the lower chord as shown in Figure 6(a). As seen from these data, the rate of recovery of the deflections was rapid initially and then diminished with time, as was noted previously during load series 1. To better define the viscoelastic behavior of the bridge, a continuous strain recovery curve was plotted with a strip-chart recorder for number 15 of the bonded strain gages. The tracing from the recorder is shown as Figure 11(b). Due to a malfunction of the recording instrumentation, the time of the complete recovery is not known and may well have been beyond the 184-hour period of the observations.

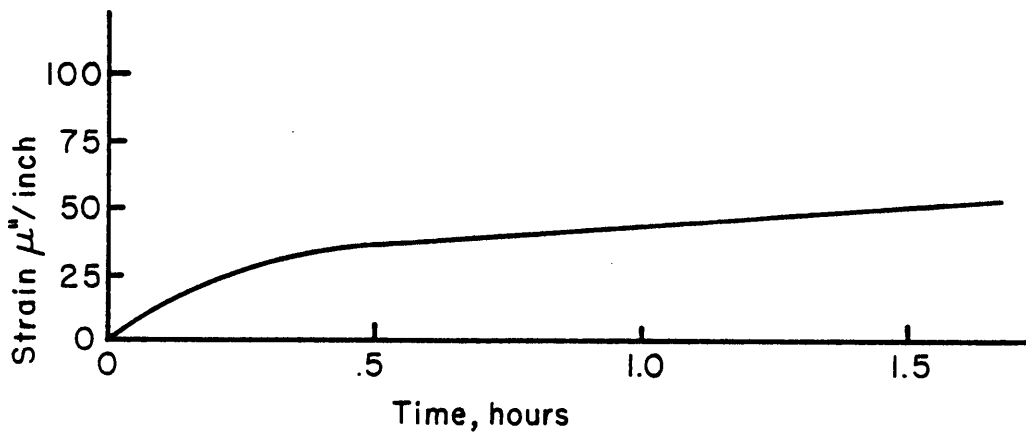
In summary, the observations of the recovery cycles indicate that the application of over 1.6 million cycles of load throughout the testing program did not significantly alter the viscoelastic recovery behavior of the bridge.

#### FAILURE MECHANISMS

Three primary failure mechanisms were identified and several conditions which might be considered a functional failure of the bridge were observed. Secondary failure modes included lower chord abrasion at the stiffener connections, delamination of the inclined web and lower chord elements, tensile and/or shear breakage of the fiberglass strands at the panel point anchorage, and separation of the flange and cover plate due to high cleavage stresses. None of these secondary failures



(a) Deflection recovery of various points



(b) Strain recovery of lower chord at gage 15

Figure 11. Viscoelastic recovery of bridge following removal of load for series 7.

had been detected during a careful inspection of the bridge upon conclusion of the fatigue testing.

Functional failures included excessive elastic deflections at design loads, viscoelastic creep into a buckled mode of the deck assembly, and residual geometric distortion of the girders upon the removal of the loads.

The three primary mechanisms were as follows:

1. Crushing of a vertical web stiffener at the north support of the east side of the west girder (see Figure 6(b) for location)
2. Formation and propagation of cracks in the adhesive joint between the flange plates and the horizontal flange stiffeners at a number of the panels in all three girders
3. Cracking through the polymer concrete wearing course and delamination of the concrete from the pultruded fiberglass flange plates

Each of the observed failure modes is discussed further in the following text.

#### Crushing of Vertical Web Stiffener

Cracks aligned parallel to the axis of one of the fiberglass tubes serving as the bearing element of the west girder were discovered on February 6, 1986, during a visual inspection of the bridge. However, it is believed that the tube first cracked on January 17, when a sudden but short-lived increase in the acoustic emission count rate was recorded. In this report, all "counts" refer to the number of acoustic emission events which occurred. The use of the term "count" is for convenience and is not to be confused with the number or "count" of the oscillations of the signal within an event. An expanded discussion of the acoustic emission data is continued on page 51. The count rate increased from less than 0.05 counts per load cycle to approximately 0.14 count per load cycle. This change was noted after 144,000 load cycles had been completed in load series 1. Additional discussion of the acoustic emission analysis is included in a later section. For the next several weeks, a clicking sound was clearly heard for each cycle of load, but the source of the sound could not be pinpointed nor related directly to the action of the bridge itself. During this time, there was no unusual change in the measurements of the deflection indicators nor of the electrical strain gages. Figure 12(a) shows the damaged stiffener in the lower right corner of the photograph. A reinforcing plate bonded to the outside stiffeners to strengthen the damaged stiffener may also be seen. Figure 12(b) is an enlargement of the cracks in one face of the stiffener tube after 378,000 load cycles on February 7, 1986.

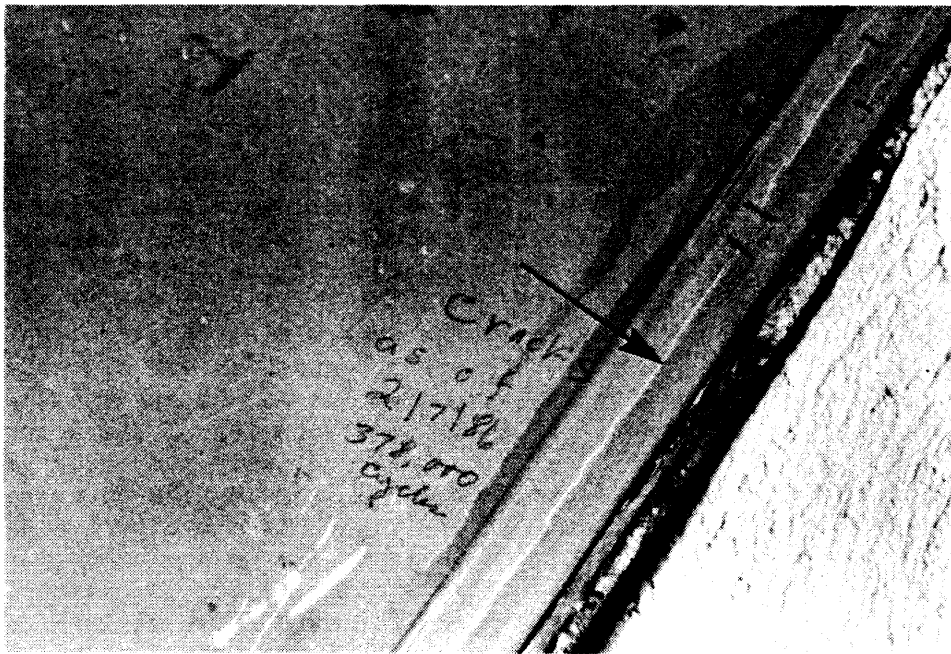
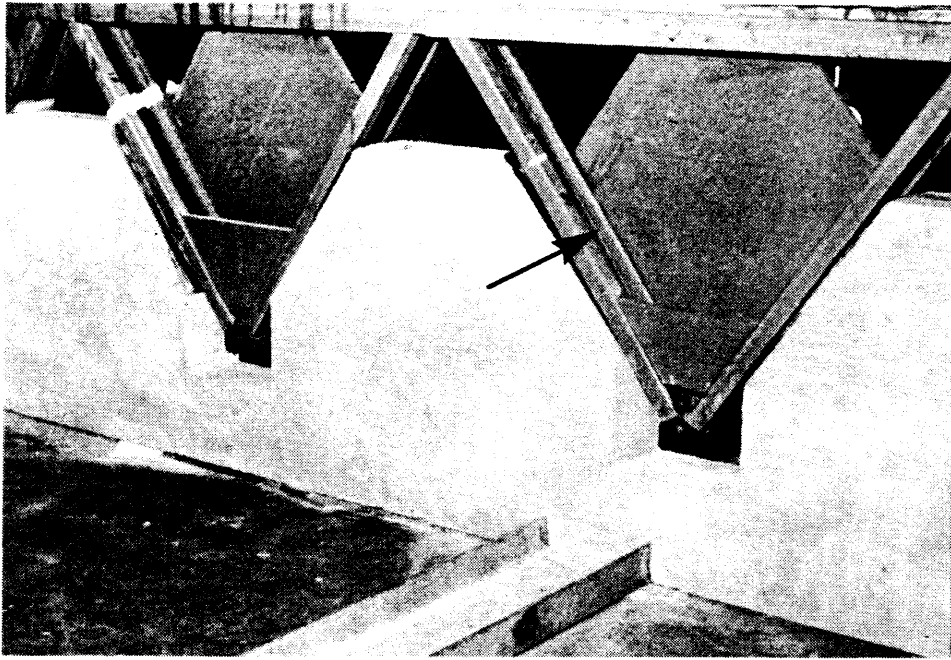


Figure 12. Flexural cracks (identified by arrow) in the face of a vertical web stiffener at a girder end support.

Estimates of the shear, bending, and bearing stresses in the stiffener at the time of crack formation revealed low values relative to the nominal strength of the composite material. Pertinent to the flexural cracks in the face of the stiffener, the calculated maximum bending stress was 1,676 psi. When compared with a nominal ultimate strength of 10,000 psi, it appears that the crack should not have formed unless the calculated estimate of the stress is incorrect or unless the stiffener had been damaged during previous handling and testing of the bridge. The prior damage hypothesis seems most plausible since none of the remaining 11 support stiffeners developed similar cracks at any time during the load test period, even though they resisted loads more than three times the value at which the cracks developed.

### Cracks in Adhesive Joints

Visible cracks in the adhesive joints between the flange plates and the horizontal stiffeners were observed at the ends of some of the stiffeners during load series 3 (1,600 to 4,000 lb load range at 9 cycles per minute). The formation of the small cracks was not unexpected since the reactive forces from the web diagonal elements were applied to the ends of the stiffeners. No cracks had been observed and no unusual change in the rate of acoustic emissions had been noted, which would suggest a new major source of emissions prior to the beginning of load series 3. However, because of the relatively large loads and displacements imposed on the structure, a careful survey was made of each joint for the presence of cracks following 100,000 cycles of load series 3. The findings from the joint survey on March 3, 1986, are shown in Table 3. Most of the cracks were hairline in dimension, as shown Figure 13. Note that the crack is wider at the end of the stiffener (right side of photograph) than it is away from the end. This crack was 2.8 in long when first observed on March 3, 1986, and did not extend further with additional load cycles. A GRP pin connecting the horizontal and vertical stiffeners is seen in the lower right corner of the photograph. Table 3 indicates that 13 of the 28 cracks identified throughout the entire bridge were found in the joints at the outside edge of the west girder. This was the same girder with the damaged stiffener at one support, but there was no clear evidence that the weakened stiffener introduced torsional distortions or otherwise redistributed the loads or affected the west girder in such a manner that the cracks would be formed preferentially as they appeared. While not documentable quantitatively, it is more likely that the outside of the west girder had been overloaded in one of the previous moves or tests at some time prior to the current fatigue load study, and that the observed cracks were an extension of preexisting microcracks. Eight additional surveys were made periodically of the number and sizes of cracks with a complete tabulation of the location and values included in Table 3. A total of 48 cracks were identified at the conclusion of the cyclic load testing on June 17, 1986.

TABLE 3

Total Length of Crack in Adhesive Joint Between Flange Plates and Horizontal Stiffeners. Values are in Inches or Zero When Omitted.

Girder*	Stiffener*	Corner* Side	Date of Survey, 1986										
			3/3	3/21	3/25	3/31	4/7	4/16	4/30	5/27	6/17		
East	1	E/S											0.5
		E/N		0.8	0.8	0.8	0.8	0.8	0.8	1.8	1.8	1.8	1.8
		W/S	1.5	1.5	1.5	1.5	1.5	1.5	1.5	1.5	1.5	1.5	1.5
		W/N	2.3	2.3	2.3	2.3	2.3	2.3	2.8	2.8	2.8	2.8	2.8
	2	E/S			1.0	1.0	1.0	1.0	1.8	1.8	1.8	1.8	1.8
		E/N											
		W/S											
		W/N											
	3	E/S											
		E/N											
		W/S											
		W/N											
	4	E/S											
		E/N											
		W/S											
		W/N											
	5	E/S											
		E/N											
		W/S											
		W/N											
	6	E/S											
		E/N	0.5	0.5	0.5	0.5	0.5	0.5	0.5	0.5	0.5	0.5	1.5
		W/S		1.3	1.3	1.3	1.3	1.3	1.3	1.3	1.3	1.3	1.3
		W/N											
	7	E/S											
		E/N											
		W/S											
W/N													
8	E/S	1.0	1.0	1.0	1.0	1.0	1.0	1.0	1.0	1.0	1.0	1.0	
	E/N	1.0	1.0	1.0	1.0	1.0	1.0	1.0	1.0	1.0	1.0	1.0	
	W/S			0.7	0.7	0.7	0.7	0.7	0.7	0.7	0.7	0.7	
	W/N												
9	E/S	1.8	1.8	1.8	1.8	1.8	1.8	1.8	2.0	2.0	2.0	2.0	
	E/N	2.5	2.5	2.5	2.5	2.5	2.5	2.5	2.5	2.5	2.5	2.5	
	W/S								0.5	0.5	0.5	0.5	
	W/N												

\* See Figure 6(b) for key to nomenclature.

TABLE 3 continued

<u>Girder*</u>	<u>Stiffener</u>	<u>Corner*</u> <u>Side</u>	<u>Date of Survey, 1986</u>									
			<u>3/3</u>	<u>3/21</u>	<u>3/25</u>	<u>3/31</u>	<u>4/7</u>	<u>4/16</u>	<u>4/30</u>	<u>5/27</u>	<u>6/17</u>	
Middle	1	E/S	4.0	4.5	4.5	4.5	4.5	4.5	4.5	4.5	4.5	4.5
		E/N	4.0	4.0	4.0	4.0	4.0	4.0	4.0	4.0	4.0	4.0
		W/S										
		W/N										
	2	E/S										
		E/N										
		W/S										
		W/N										
	3	E/S										
		E/N										
		W/S										
		W/N										
	4	E/S										
		E/N										
		W/S							1.4	1.4	1.4	
		W/N										
	5	E/S										
		E/N		0.8	0.8	0.8	0.8	0.8	0.8	0.8	0.8	0.8
		W/S										
		W/N										
	6	E/S										
		E/N										
		W/S	3.8	3.8	3.8	3.8	3.8	3.8	3.8	3.8	3.8	4.0
		W/N	2.8	2.8	2.8	2.8	2.8	2.8	2.8	2.8	2.8	2.8
7	E/S											
	E/N											
	W/S											
	W/N											
8	E/S					1.0	1.0	1.0	1.0	1.0	1.0	
	E/N		0.5	0.5	0.5	0.5	0.5	0.5	0.5	0.5	0.5	
	W/S										2.0	
	W/N	1.5	1.5	1.5	1.5	1.5	2.3	2.3	2.3	2.3	2.3	
9	E/S	4.0	4.0	4.0	4.0	4.0	4.0	4.0	4.0	4.0	4.0	
	E/N	1.3	3.5	3.5	3.5	3.5	3.5	3.5	3.5	3.5	3.5	
	W/S											
	W/N	0.8	0.8	0.8	0.8	0.8	0.8	0.8	0.8	0.8	0.8	

TABLE 3 continued

Girder*	Stiffener	Corner* Side	Date of Survey, 1986										
			3/3	3/21	3/25	3/31	4/7	4/16	4/30	5/27	6/17		
West	1	E/S		2.5	2.5	2.5	2.5	2.5	2.5	2.5	2.5		
		E/N											
		W/S											0.5
	2	W/N	2.8	2.8	2.8	2.8	2.8	2.8	2.8	2.8	2.8	2.8	2.8
		E/S											
		E/N											
	3	W/S		1.5	1.5	2.0	2.0	2.0	2.0	2.0	2.0	2.0	2.0
		W/N											
		E/S											
	4	E/N											
		W/S	0.8	0.8	0.8	0.8	0.8	0.8	0.8	0.8	0.8	0.8	0.8
		W/N	2.3	2.3	2.3	2.3	2.4	2.4	2.4	2.4	2.4	2.4	2.4
	5	E/S											
		E/N											
		W/S	0.5	0.5	0.5	0.5	0.5	0.5	1.5	1.5	1.5	1.5	1.5
	6	W/N		0.5	0.5	0.5	0.5	1.5	1.5	1.5	1.5	1.5	1.5
		E/S											
		E/N											
	7	W/S	0.5	0.5	0.5	0.5	0.5	0.5	0.5	0.5	0.5	0.5	0.5
		W/N	0.5	0.5	0.5	0.5	0.5	0.5	0.5	0.5	0.5	0.5	0.5
		E/S											
	8	E/N											
		W/S0	0.5	0.5	0.5	0.5	0.5	0.5	0.5	0.5	0.5	0.5	0.5
		W/N	0.8	0.8	0.8	0.8	0.8	0.8	0.8	0.8	0.8	0.8	0.8
	9	E/S											
		E/N											
		W/S	1.5	1.5	1.5	1.5	1.5	1.5	1.5	1.5	1.5	1.5	1.5
10	W/N	1.3	1.3	1.3	1.3	1.3	1.3	1.3	1.3	1.3	1.3	1.3	
	E/S												
	E/N		0.5	0.5	0.5	0.5	0.5	0.5	0.5	1.0	1.0	1.0	
11	W/S	1.3	1.3	1.3	1.3	1.3	1.3	1.3	1.3	1.8	1.8	1.8	
	W/N	1.3	1.3	1.3	1.3	1.3	1.3	1.3	1.3	1.3	1.3	1.8	
	E/S												
12	E/N	2.0	2.0	2.0	2.0	2.0	2.0	2.0	2.0	2.3	2.3	2.3	
	W/S	1.5	1.5	1.5	1.5	1.5	1.5	1.5	1.8	1.8	2.0	2.0	
	W/N	2.0	2.0	2.0	2.0	2.0	2.0	2.0	2.0	2.0	2.0	2.0	



Figure 13. Typical crack in adhesive joint between flange plate and horizontal stiffener.

It was anticipated that the cracks in the adhesive joints would extend more than they did under the action of the cyclic loads. As stated previously, the relatively large loads and deflections of series 7 were purposely selected to accelerate crack development in the adhesive bonding the horizontal stiffeners to the flange plates of the girders. The fact that little additional damage was noted in the joints during the half-million cycles of loads applied during series 7 speaks well of the general fatigue resistance of the bridge; i.e., the toughness of the composite material and the ability of the joints and elements to distribute overloads internally as needed to equalize stresses throughout the structure. While there was no way to assess the behavior directly, it is probable that the small (1/4-in diameter) metallic machine bolts installed at each end of the horizontal stiffeners prevented the development of excessive cleavage stresses in the stiffener-flange plate connections. Experience had determined that under service loads imperceptible torsional distortion of the girders (along their longitudinal axes) generated destructively high tensile cleavage stresses in the joints and resulted in failures of the joint at very low computable shear stresses. For this reason, the small bolts had been used to minimize the cleavage stresses in the current test structure, and from the test results this design feature appears to have been quite successful.

#### Polymer Concrete Wearing Course

The polymer concrete wearing course was applied to the cover plate of the bridge deck in the spring of 1985. A nominal thickness of 1/2 in was built up by successive applications of 1/8 in thick layers of silica sand and polyester binder (Reichhold Chemical Polylyte 92-339). No primer nor other type of interfacial coupling agent was used between the first resin layer of the concrete and the surface of the plate. Compressive tests of both cylinders and prisms of samples of the polymer concrete materials indicated that the 24 hour room temperature compressive strength was 7,100 psi with a standard deviation of 390 psi. The tests also indicated a Poisson's ratio of -0.25 at 73°F and that the compressive modulus of elasticity increased as the test temperature decreased. A value of  $1.25 \times 10^6$  psi for the compressive modulus was considered appropriate for the material in the bridge deck, since the temperature and relative humidity of the testing laboratory remained at approximately 78°F and 50%, respectively, throughout the test period.

Several times during the fatigue test program wearing course was inspected visually for surface cracks, but none were found. An effort was made to determine the integrity of the bond at the interface by tapping the surface with a light hammer and listening for a difference in sound from point to point. Again, no evidence of delamination was apparent. A third determination of the interfacial bond was made by means of ACI test procedure 503R, wherein 2 in diameter cores were drilled through the wearing course and subjected to an ultimate tensile test. Figure 14 shows the location of the cores on a plan view of the

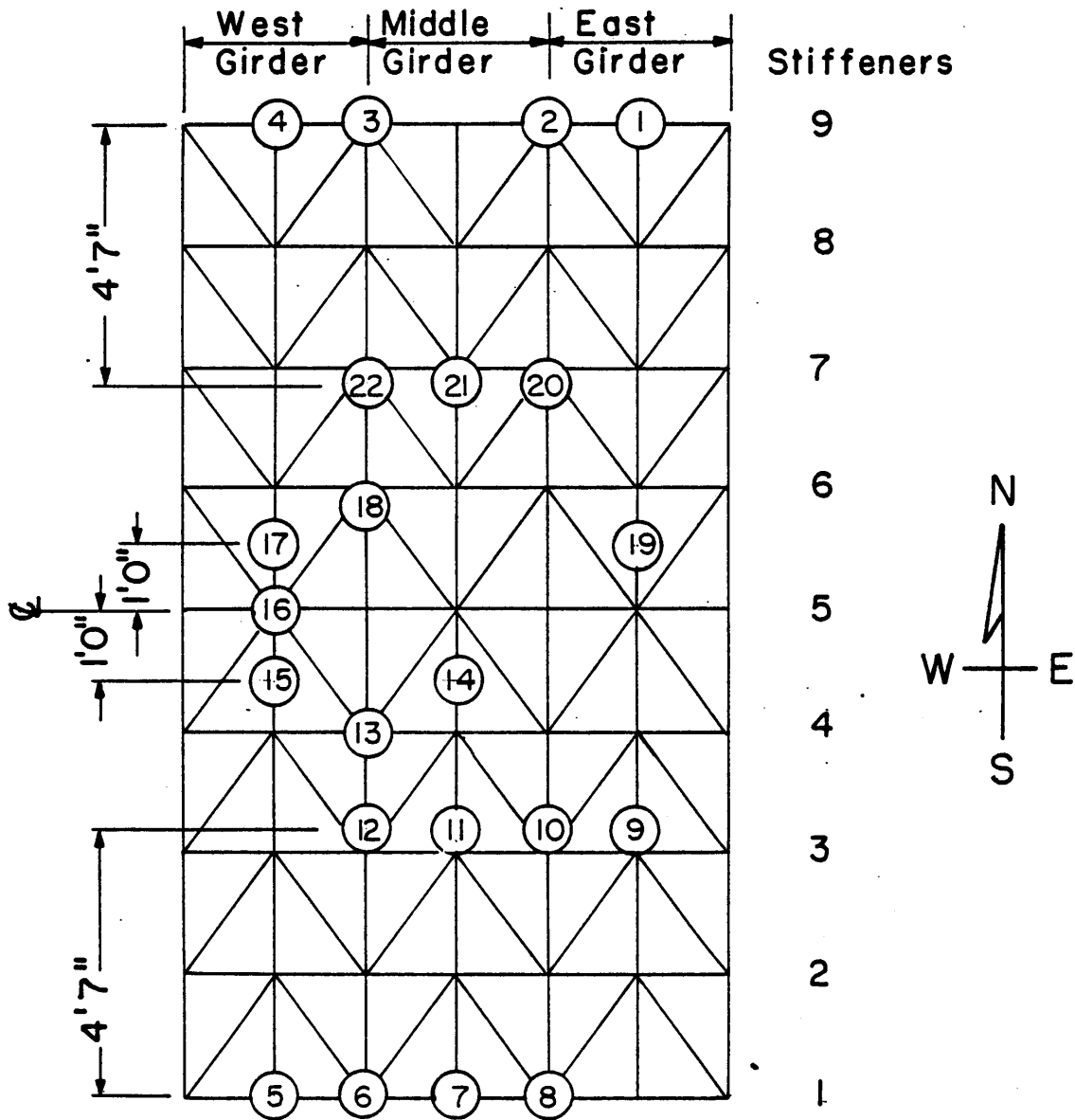


Figure 14. Location of cores drilled through the polymer concrete wearing course for tensile bond test.

deck. Figure 15 shows the tensile test fixture loading a core and Figure 16 identifies typical fracture surfaces listed in Table 4. Table 4 presents the tensile strength data measured for each core.

Cores 1 through 8 were located within an area of the deck which presumably was unaffected by the application of the cyclic loads. These cores were intended to provide a reference strength for subsequent tests. The centers of the cores were located between the ends of the deck and the end stiffeners, which transmitted the reactions from the supports to the deck. However, in view of the large distortions and possible damage the bridge had undergone during removal from the previous test location in Pen Park, the cores were selectively located to ascertain if bond strengths differed between girder-joint areas and areas away from the joints. The average rupture strengths,  $\bar{x}$  for the reference cores were as follows:

3 cores over joints:  $\bar{x} = 387$  psi,

4 cores away from joints:  $\bar{x} = 629$  psi.

While the strength of the material over the joints apparently was lower than that of the other material, the modes of failures of the various cores do not provide conclusive evidence of preferential degradation of strength at the joint locations. For example, both cores 5 and 8 experienced failure predominantly at the interface and core 3 had a smaller interfacial failure area than core 1. While most of the failures at the interface of the polymer concrete and the GRP cover plate revealed few air voids, the surface at core 6 had a large area over which no resin was applied. Several of the fracture surfaces also included small patches of the GRP plate which had failed just beneath the fill coat of the composite. Thus, it is not known whether the variation in the core strength was due to prior damage to the structure or represents a normal distribution of strengths in the materials for this type of installation.

The locations of cores 9 through 22 were distributed over the loaded area of the deck to determine if the action of the repeated loads had degraded the bond of the polymer concrete to the GRP cover plate. As in the data from cores 1 through 8, there was considerable variation in the tensile strengths of the cores. Several failures occurred between the epoxy adhesive and the surface of the steel cap. In addition, the strength of two cores exceeded the capacity of the test fixture. From an analysis of the test data, the average bond strength of the wearing course over the joints between girders was greater than 475 psi and the average strength in the material away from the joints was greater than 467 psi. From these values, it does not appear that the strength of the polymer concrete wearing course was adversely affected by the presence of joints between the girders, and that the 1/4 in thick cover plate was adequate to successfully transmit the shear and flexural stresses generated throughout the bridge deck.

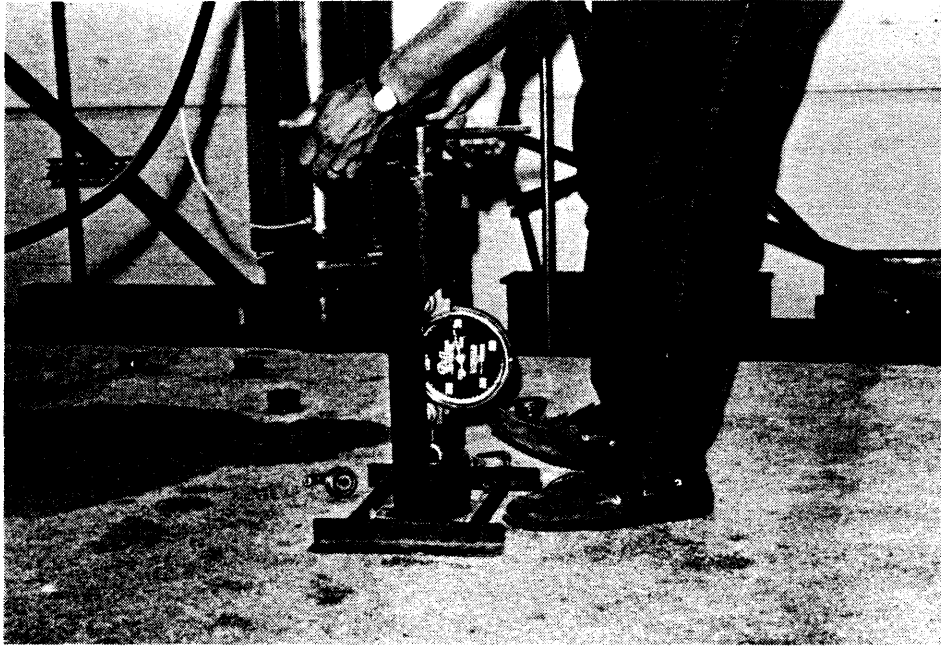


Figure 15. Tensile test fixture applying a force to a 2-in diameter core in the polymer concrete wearing course.

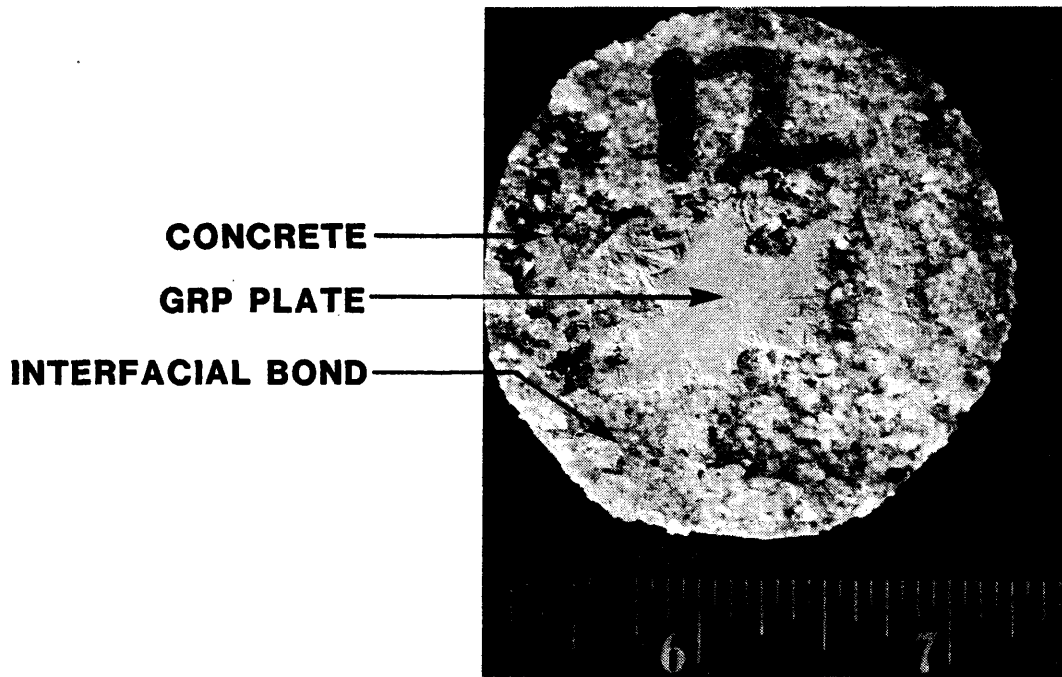


Figure 16. Representative fracture surfaces on core 12 showing different types of failures.

TABLE 4

## Tensile Strength of Cores in Polymer Concrete Wearing Course

Core No.	Rupture Force, lbf	Rupture Stress, psi	Failure Mode,* % of Area
1	2,150	684	25% bond, 75% concrete
2	0	N/A	Broken in preparation
3	1,650	525	15% bond, 85% concrete
4	2,050	653	100% concrete
5	1,500	477	90% bond, 10% concrete
6	1,200	382	30% cover and plate, 70% voids
7	2,200	700	75% bond, 7% concrete
8	800	255	98% bond, 5% concrete
9	1,400	455	85% bond, 15% concrete
10	2,000	637	33% each bond, concrete, plate
11	1,500	427	50% bond, 50% concrete
12	1,250	398	80% bond, 10% concrete, 10% plate
13	1,600	509	Cap
14	2,500	796	Exceeded capacity of fixture
15	2,500	796	Exceeded capacity of fixture
16	1,350	430	60% bond, 40% concrete
17	1,500	477	Cap
18	1,700	541	80% bond, 10% concrete, 10% plate
19	1,850	589	40% bond, 60% concrete
20	1,200	382	50% bond, 50% concrete
21	1,200	382	100% bond at top of course
22	1,200	382	100% concrete

\*Abbreviations: "bond" refers to interfacial bond at surface of cover plate; "concrete" refers to failure within the polymeric concrete layer; "plate" refers to failure within the fiberglass cover plate; "cap" refers to bond failure of the cap to the concrete.

A further consideration of the strength results from cores 9 through 22 and those from cores 1 through 8 does not indicate that the cyclic action of the loads degraded the wearing course in any way. The lower elastic modulus of the polymer concrete relative to that of the GRP cover plate undoubtedly relieved the concrete from developing high stresses at the interface which would result in eventual debonding and a loss of tensile strength.

It is interesting to note that cores 4 and 22 both exhibited a rupture surface entirely within the polymer concrete, which presumably established the in-place tensile strength of this material with a range from 382 to 653 psi. However, cores 14 and 15 both exceeded a strength of 796 psi without failure, which also is indicative of the strength of the concrete material. This wide variation in the measured tensile strengths of the polymer concrete emphasizes the inherent variability in the properties of the material, and the variability of the bond strength at the interface with the plate.

#### Acoustic Emission Results and Interpretations

Throughout the cyclic load investigation, close attention was given to the rate and character of the acoustic emissions (AE) produced by the bridge. It was anticipated that the formation of new cracks or extensive propagation of existing cracks would result in large spikes in the rate of emission data. In accordance with contemporary AE theories and interpretations, it was also anticipated that the decibel amplitudes of the emissions would increase with progressive rupture of the composite material, as contrasted with the low energy of the emissions generated by the rubbing action of existing cracks or other surfaces.

Earlier discussion of the failure of the vertical web stiffener (page 27) alluded to some of the AE data obtained during load series 1. A summary of the complete record of the data is presented in Figure 17. An analysis of the AE data based on the extensive crack pattern in the stiffener provided some understanding of the erratic output of the AE processors. As seen in Figure 17, both the counts and count rate were practically nonexistent until the first observed spike in the count rate at 144,000 cycles (still too small to plot at the scale of Figure 17). At this point, the first crack presumably formed in the stiffener. The AE record shows another spike of 0.40 per load cycle at 246,000 cycles of load which is indicative of a significant growth in the initial crack or the formation of another crack in the stiffener. This spike is just perceptible in Figure 17. The next AE count rate spike of 5.8 per load cycle appeared at 260,000 cycles of load. Thereafter, the AE counts remained relatively quiet, with five additional count rate spikes appearing at 305, 311, 320, 338 and 352 x 10<sup>3</sup> load cycles. At 360,000 cycles, very high count rates continued, as shown plotted in Figure 17. These AE outputs indicate ongoing and irregular crack growth or rubbing between the surfaces of the newly formed cracks in the stiffener. The clicking heard prior to and for a time following the discovery of the

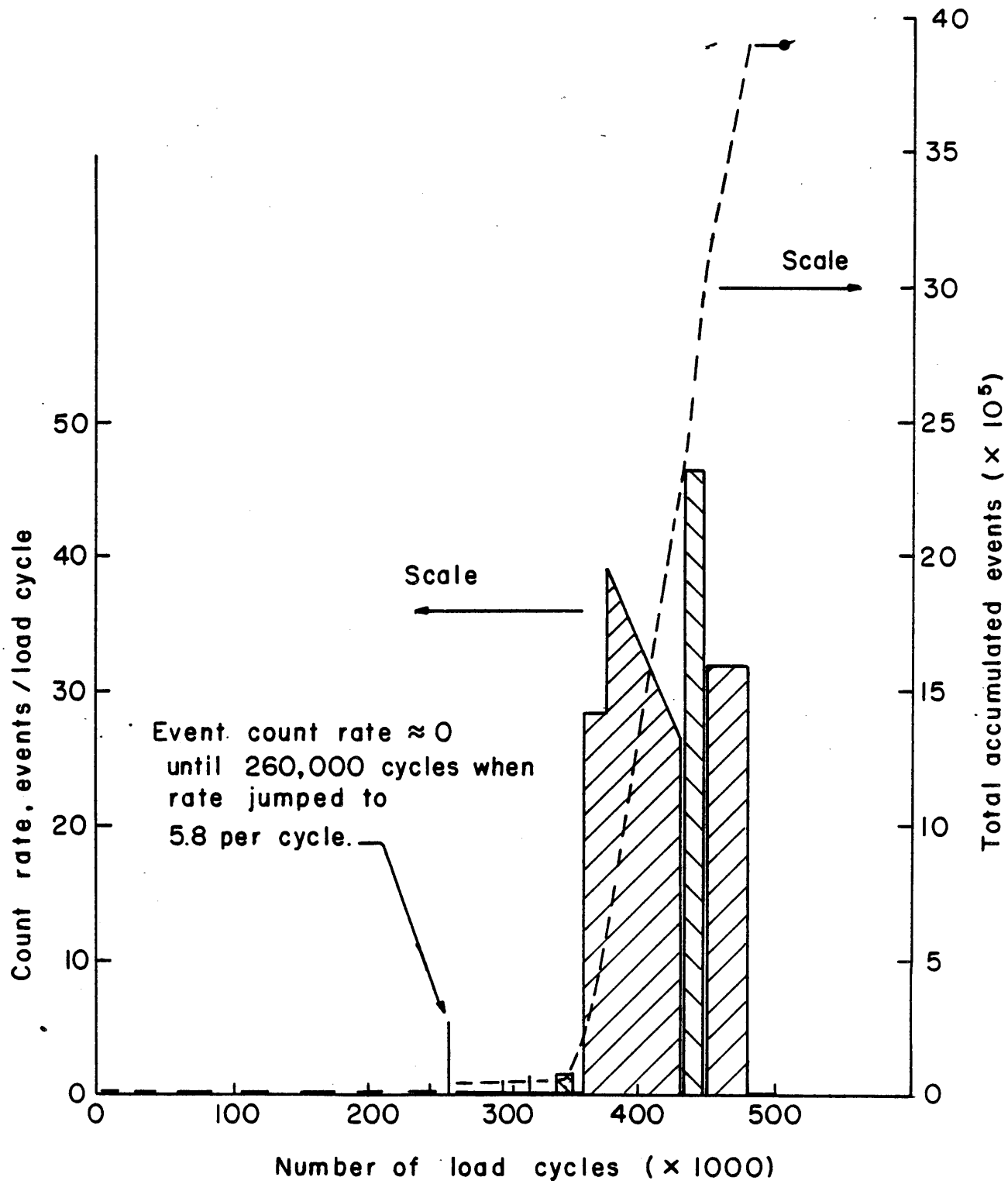
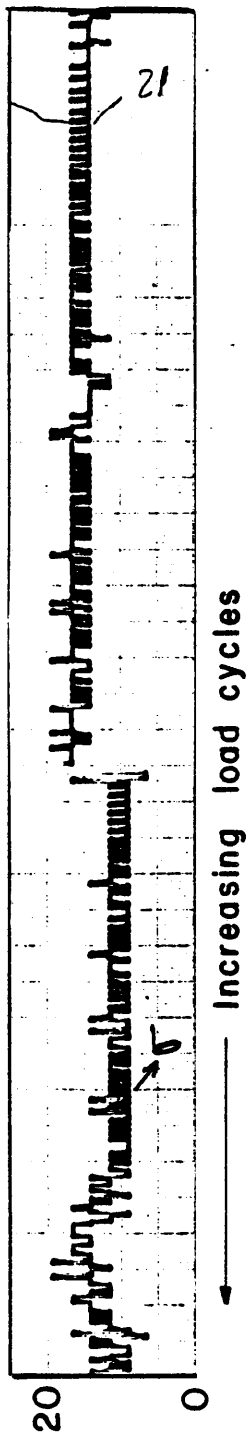


Figure 17. Acoustic emission data for load series 1.

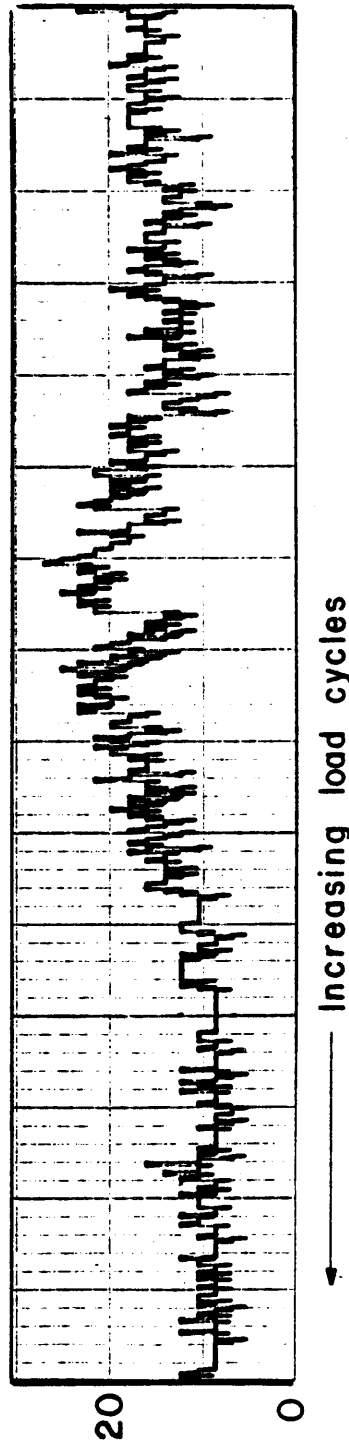
damaged stiffener may have been attributable to the rubbing action of the crack surfaces. The sound would increase and decrease in intensity for no particular reason nor at any particular time. The variations correlated, to an extent, with the observed AE count rate. While undocumented, it is now believed that the rough surfaces of new cracks produced clicks until the surfaces were polished by the cyclic motion of the loads, at which time the audible clicks and the AE counts ceased. Figure 17 also shows the accumulated number of events counted during load series 1. Note that no counts were recorded for the last 20,000 load cycles and that the total number of counts was approximately  $39 \times 10^5$ , most of which occurred after 360,000 cycles of load. Undoubtedly, the initial cracks which formed and propagated in the stiffener were so small that they escaped detection prior to the damage which occurred at 360,000 cycles and beyond.

Other than the sudden change in the count rate associated with the failure of the support during load series 1, there were no dramatic changes in the AE records attributable to the generation of cracks in the flange plate/stiffener joints. Multiple emissions per cycle continued regularly during each load application, with the emission rates ranging, on average, from 1 to 4 per load cycle. Compared with the peak rate of over 46 per load cycle during series 1, the number of emissions generated by the joint failures and other sources indicated that damage to these elements was relatively low.

Figure 18 presents representative copies of strip chart plots of the AE counts vs time for load series 5 and 6. Figure 18(a) depicts a relatively quiet period of emissions recorded during series 5 when the count rate was quite regular over a considerable length of time. The data shown in Figure 18(a) are typical of those expected from emissions originating from machine noise or surfaces rubbing together at a relatively constant energy level. Figure 18(b) was taken from the record of load series 6 after 15,200 cycles. These data are typical of a periodically fluctuating rate of emissions which characterized much of the recordings made during load series 6 and 7. Figures 18(a) and 18(b) are directly comparable since the cyclic load rates were 5 per minute in both cases. Note that the spread of the count rate band increased somewhat from load series 5 (3 counts/min) to load series 6 (6 counts/min) in addition to the fluctuating oscillation of the band. Figures 19(a) and 19(b) were taken from emission count rate data for load series 7 and represent the extremes in "quiet" and "noisy" periods of emissions observed throughout the period of cyclic loading. Figure 19(a) depicts a narrow count rate band with a nearly constant emission rate of 2.8 counts per cycle (computed from 28 counts/min at a load rate of 10 cycles/minute) which extended over a period of 15 hours. Figure 19(b) depicts widely fluctuating count rates over relatively short periods of time and large changes in the count rate magnitudes. Count rates varied from a low of 1 to a high of 7 per load cycle within a period of 10 hours. It is significant that the chart record of Figure 19(b) occurred near the beginning (13,000 cycles) of load series 7, whereas the record of Figure 19(a) was taken after 175,000 cycles of load. An inspection



(a) Typical emissions throughout load series 5



(b) Emissions from load series 6 after 15,200 load cycles

Figure 18. Representative acoustic emission rates for load series at a load rate of 5 cpm.

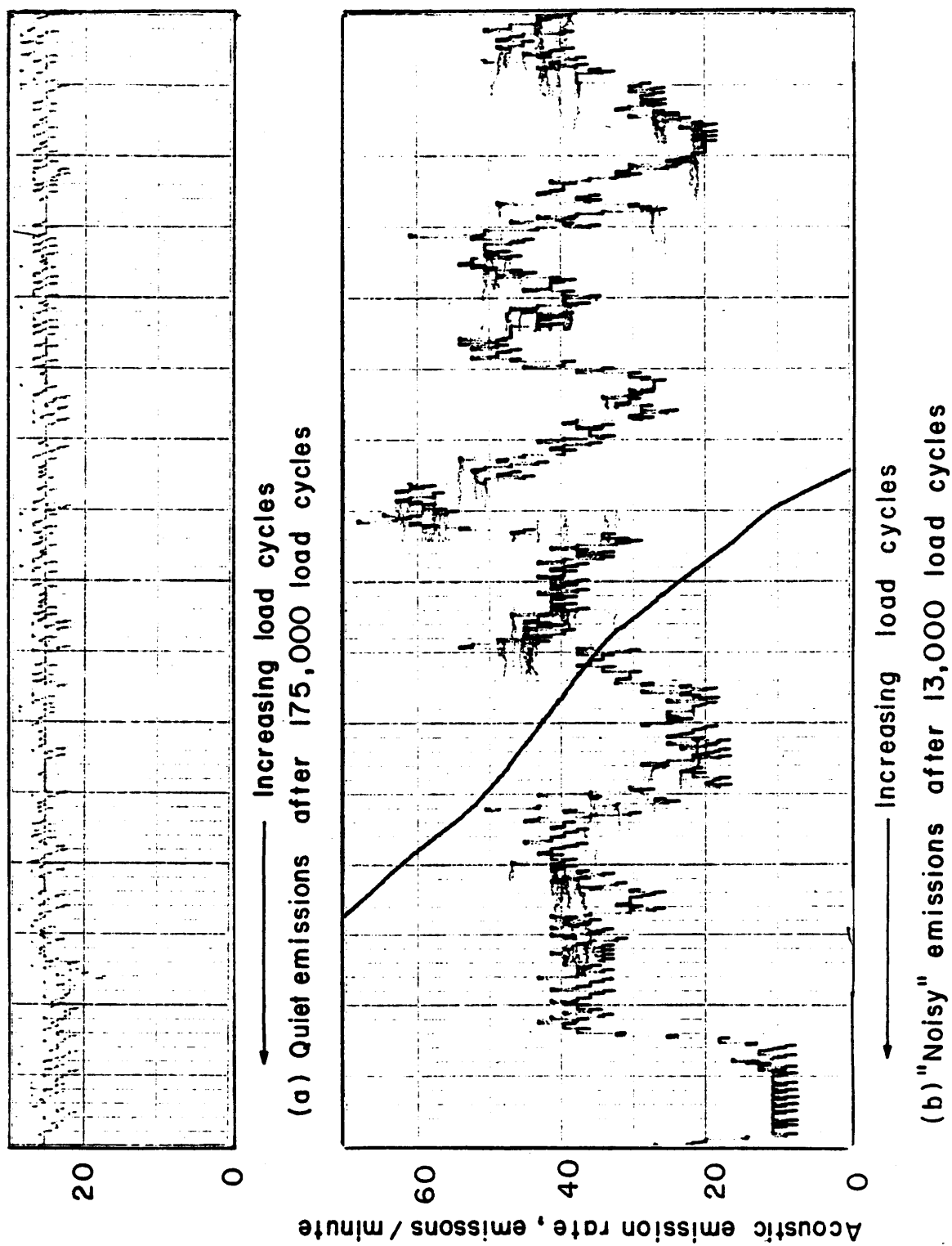
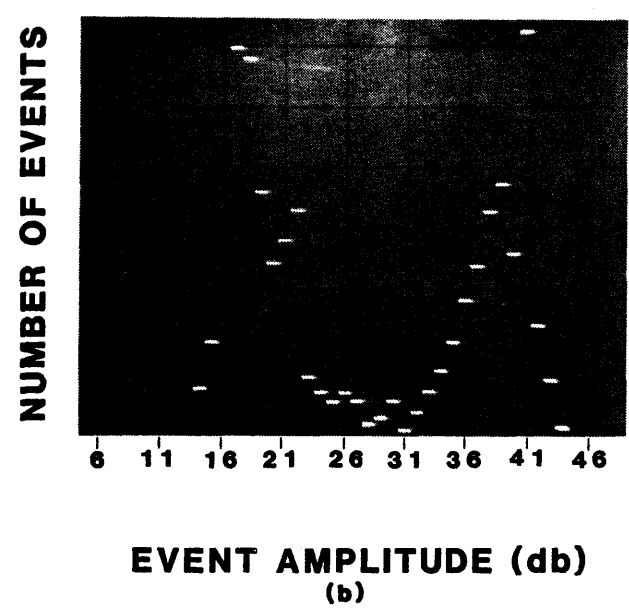
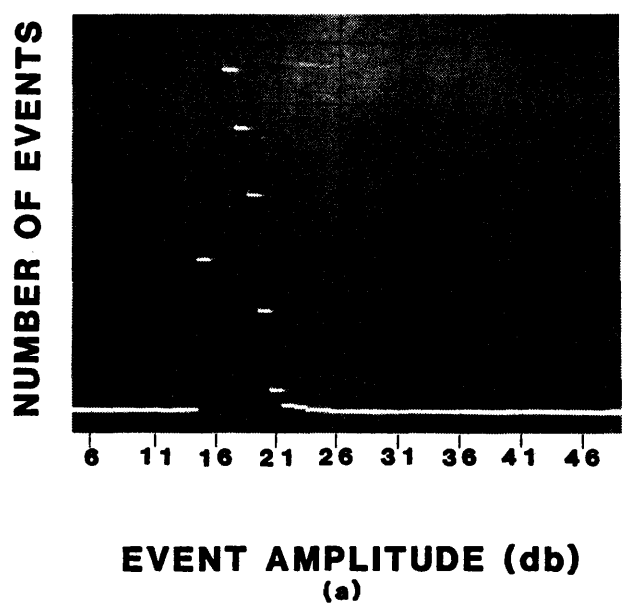


Figure 19. Typical acoustic emission rates during load series 7.

of AE data from both load series 5 and 6 revealed the same information; the count rate at the start-up period of the load series was significantly higher and more variable than the rates which occurred as the load test progressed. These observations support the deflection data discussed previously and support the contention that the bridge underwent a shakedown each time a load magnitude or distribution was changed. During this time new cracks would be formed or old ones would be extended as the structure shifted loads from one element to another and attempted to adjust to a different stress and displacement environment. After the period of adjustment, the structure would respond to the cyclic loads with a diminished rate of crack formation and extension and with fewer emissions.

Along with observed fluctuations in the emission count rate, the peak intensity of each emission was indicated by the amplitude distribution analyzer. Several representative traces from the cathode-ray screen of the instrument are included in Figure 20. The peak amplitudes of the AE counts are shown in units of decibels (dB) on the energy scale (abscissa) and in number of counts (ordinates) for each of the dB channels. The energy scale of the instrument extended from 0 to 60 dB (corresponding to 10 mv and 10 v, respectively) and each channel held a maximum number of 1,023 counts. The presentation of the traces are intended only to show variations in the predominance of the energy levels of the AE emissions and are not to be compared on a numerical basis. A threshold setting of approximately 10 dB eliminated from the screen the low energy counts attributed to background noise in the laboratory. The image presented in Figure 20(a) was taken during load series 4 after the completion of 101,111 load cycles and was typical of the low energy emission attributed to surface rubbing. Figure 20(b) shows a bimodal distribution of counts which indicate considerable activity on both ends of the energy scale. This distribution may be related to a period of loading in which a combination of surface rubbing and crack formation and extension occurred in the structure. This trace was produced following the completion of 30,000 cycles in load series 6. Figure 20(c) is the trace taken from an oscilloscope screen of an AE "burst" which defines the amplitude and the decay time of the emission signal for a discrete count. For the recording shown, the horizontal scale was 1 ms/div. and the vertical scale 5 V/div. As can be seen, two counts were emitted from the same or different locations in the bridge within the 10 ms required for the electron beam to sweep the oscilloscope screen.

Figure 21(a) is a record of the amplitude distribution of counts during load series 7 after 380,200 cycles of load ranging from 6,400 to 9,040 lb. Figure 21(b) is a view of the emissions recorded approximately two hours earlier when the load range was 6,320 to 8,400 lb. Other test conditions were essentially the same for the emission displays recorded. The change in the character of the emissions from Figure 21(a) to 21(b) is a demonstration of the phenomenon known as the Felicity effect in AE technology. In this particular case, the pattern of emissions indicate that a reduction in the mean load magnitude on the bridge



- (a) Amplitude distribution for machine noise and surface rubbing.
- (b) Amplitude distribution of events including surface rubbing, matrix cracking and some fiber breakage.
- (c) Typical envelopes of two events occurring within a period of 2 millisecc.

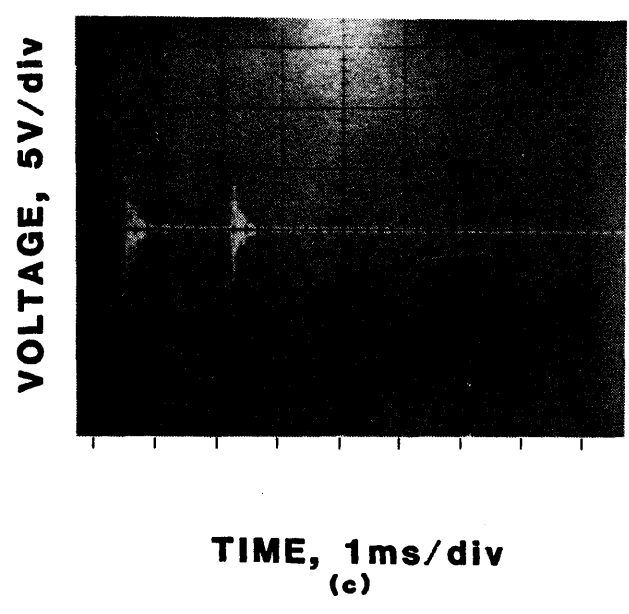
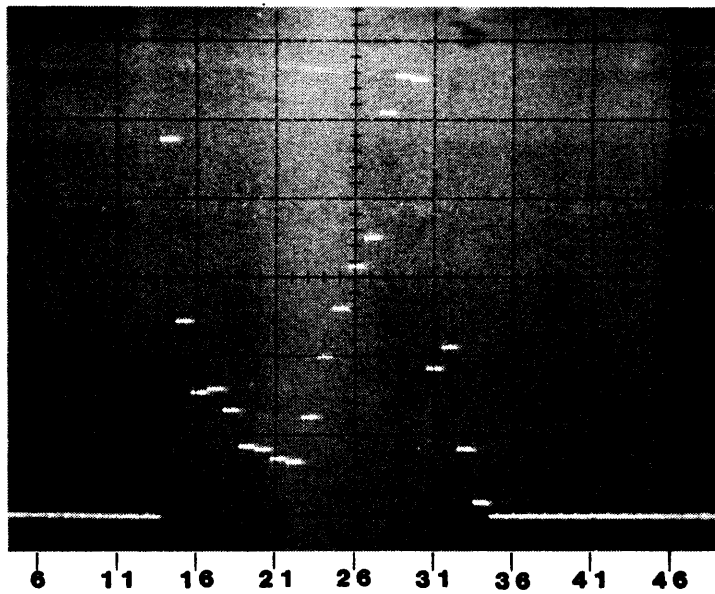


Figure 20. Typical acoustic emission traces.

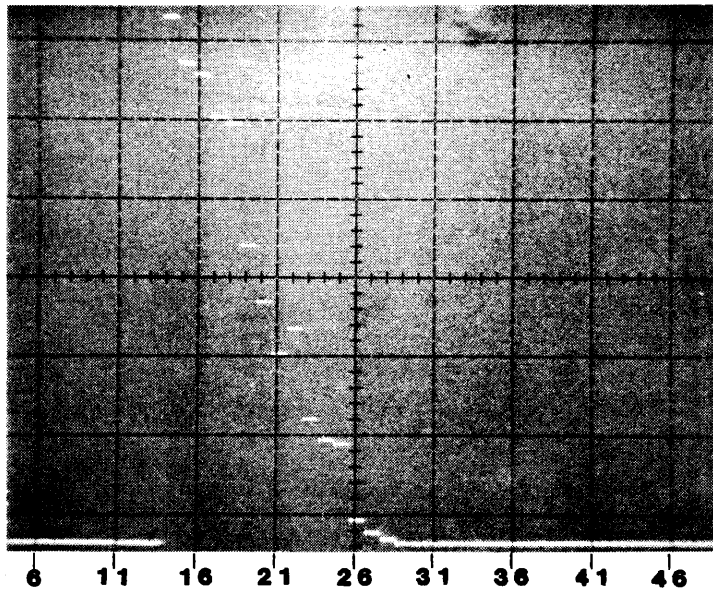
NUMBER OF EVENTS



EVENT AMPLITUDE (db)

(a) Bimodal trace of events with amplitudes to 34 db cyclic load range from 6,400 to 9,040 lb.

NUMBER OF EVENTS



EVENT AMPLITUDE (db)

(b) Emission at cyclic load range of 6,320 to 8,400 lb showing psuedo Kaiser effect of high db values produced in (a).

Figure 21. Amplitude distribution of acoustic emissions from load series 7.

terminated, at least momentarily, the production or extension of high-energy, emission-generating cracks. A corresponding dramatic drop in the total emission count rate is also noted with a decrease in load effort. For example, a mini experiment was conducted in which the load range was 6,440 to 8,800 lb and the count rate averaged 40/min. When the load range was dropped to 6,400 to 8,480 lb, the count rate went to zero for several minutes. The experiment was conducted after the completion of 400,000 cycles of load series 7 and the structure was beyond the shake down period.

The overall data provided by the AE record (and verified by the periodic visual crack surveys of the bridge) indicated that crack formation and extension was progressive and random with cyclic loading. The data also indicate that the count rate was due principally to microcracks, since the macrocracks did not increase drastically throughout the entire cyclic load program.

#### ULTIMATE STATIC LOAD TEST

A static load was applied to the bridge to determine the maximum value obtainable and the manner in which the structure would fail. The load was applied with the same arrangement as cyclic load series 6 and 7. The maximum total load was 16,640 lb, which was applied in ten increments of 1,600 lb. Six of the bonded strain gages were monitored and nine deflection indicators were used to observe displacements of the bridge deck throughout the load test. An AE record was made of the test by means of a single sensor mounted on the center horizontal stiffener of the middle girder.

#### Structural Failures

The first indication of a major failure occurred with a load of 14,000 lb, when the bridge emitted a loud sound. However, there was no drop in the load indicator of the testing machine until a load of 16,140 lb was reached. At that time, another loud sound similar to a shotgun blast was heard, and the north end of the west girder sagged considerably. The load indicator dropped to approximately 12,000 lb but recovered to 14,000 lb before the test was terminated. Upon inspection, it was determined that both ends of the inside horizontal stiffener on the northwest end of the west girder had cracked and one end was displaced forward approximately 1 in. The attached vertical web stiffener was bent, but not broken. The bond joint between the stiffener and the flange plate was ruptured for a distance of 5 in from both ends of the stiffener. However, the joint remained intact along the center 18 in of its length. A similar but less severe failure, occurred in the horizontal stiffener of the middle girder at the north end of the bridge. It was apparent that the failures of the stiffeners resulted from the large forces developed in the attached web diagonals.

The experimental verification of the linear load-deflection relationship validated the use of this assumption in constructing the mathematical model for the theoretical analysis of the bridge.

It was anticipated that cracks would form in the longitudinal joint between the girders. Only one panel was found to have developed such cracks. This panel was located in the east girder and adjacent to the end panel of the north end (see Figure 6). It could not be determined whether this crack formed before or after the failure of the stiffeners in the middle and west girders. It was also observed that some of the preexisting cracks formed during cyclic load tests were extended or widened as a result of the ultimate load application.

No evidence of cracking nor spalling of the polymer concrete wearing course was obtained from a visual examination of the deck surface.

#### Deflection Measurements

The maximum net deflection of the top surface of the deck at the center of the bridge was 1.41 in at a load of 16,000 lb, with a correction of 0.05 in for the deflection of the supports. Figure 22 shows the measured and analytical deflections of the longitudinal and transverse centerlines of the bridge at a total load of 9,600 lb. This load value corresponds to the total nominal load ( $85 \text{ lb/ft}^2$ ) for which the bridge was designed. The analytically predicted deflections of the deck based on a uniformly distributed load are also shown for comparison in Figure 22. Table 5 presents the experimental deflection data and Table 6 presents a comparison of the experimental and analytical data for the total load of 9,600 lb.

Figure 23 graphically presents the experimental deflection data as a function of load. With the exception of the extreme edges of the bridge (gages 20 and 24), the linearity of the load deflection curves for the bridge from zero to the ultimate load is considered to be remarkable in view of the anticipated movement and rotation of the connections and joints throughout the structure. From the data of Table 5, it is apparent that the load resistance of the girders must have been quite uniform throughout the test to produce closely similar deflections at corresponding points of symmetry in the structure.

#### Strain Measurements

Continuous monitoring of the two most highly strained elements in previous tests (gage 6 on a web element and gage 15 on a chord element) provided information on the manner in which the members deformed during the load application. No unusual occurrences were noted in the data from these two gages which reached strains of 1,205 and 1,650  $\mu\text{in/in}$  at a load of 16,000 lb in the chord and web elements, respectively. Converted to unit stress, the maximum values at the ultimate load on the bridge reached approximately 8,500 psi in the chord and 12,000 psi in the web.

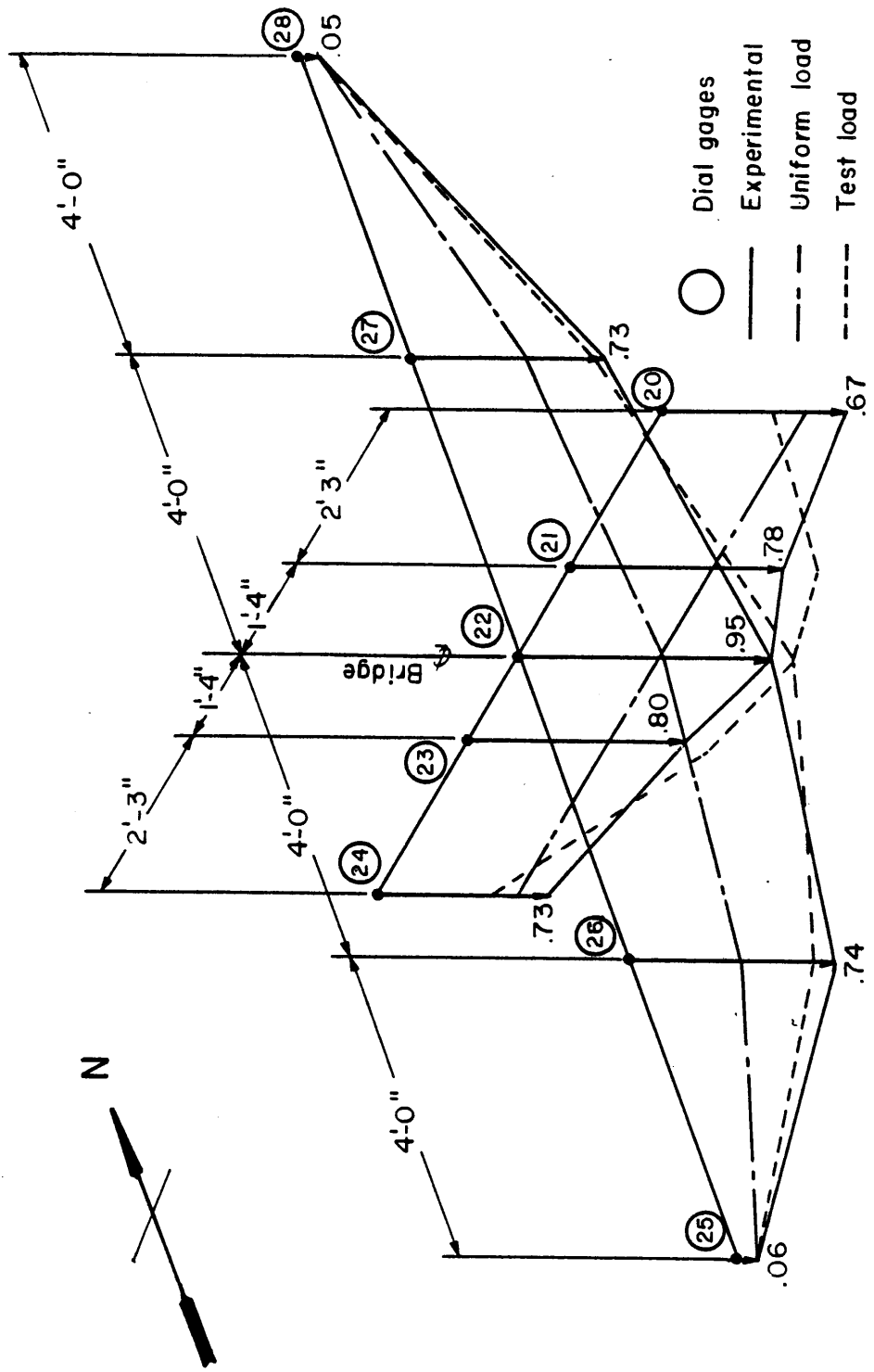


Figure 22. Deflections of bridge deck at load of 9,600 lbs.

TABLE 5

Net Deflections of Deck Surface During Ultimate Static Load Test for  
Gage Locations Shown in Figure 22

Load, lb	Gages						
	20 in	24 in	21 in	23 in	26 in	27 in	22 in
1,600	0.09	0.10	0.12	0.12	0.11	0.10	0.15
3,200	.21	.23	0.25	0.25	.23	.23	0.29
4,800	.31	.34	0.36	0.34	.34	.34	0.42
6,400	.41	.45	--	0.60	.45	.45	0.57
8,000	.51	.56	--	0.65	.56	.56	0.70
9,600	0.62	0.58	0.73	0.75	0.69	0.68	0.90
11,200	off scale		0.85	0.87	off scale		0.97
12,800	"	"	0.98	1.00	"	"	1.11
14,400	"	"	1.10	1.12	"	"	1.24
16,000	"	"	1.24	1.28	"	"	1.41

TABLE 6

Experimental and Analytical Deflections of Deck Surface for a Load  
of 9,000 lb.

Gages	Experimental Data, in	Analytical Data			
		Applied Load		Uniformly Distributed	
		Value, in	Difference, percent	Value, in	Difference, percent
20	.67	0.42	- 37	.53	- 21
21	.78	0.91	+ 17	.54	- 31
22	.95	1.03	+ 8	.54	- 43
23	.80	0.91	+ 14	.54	- 32
24	.73	0.42	- 42	.53	- 27
25	.06	0.06	0	.06	0
26	.74	0.69	- 5	.41	- 45
27	.73	0.69	- 7	.41	- 44
28	.05	0.05	0	.05	0

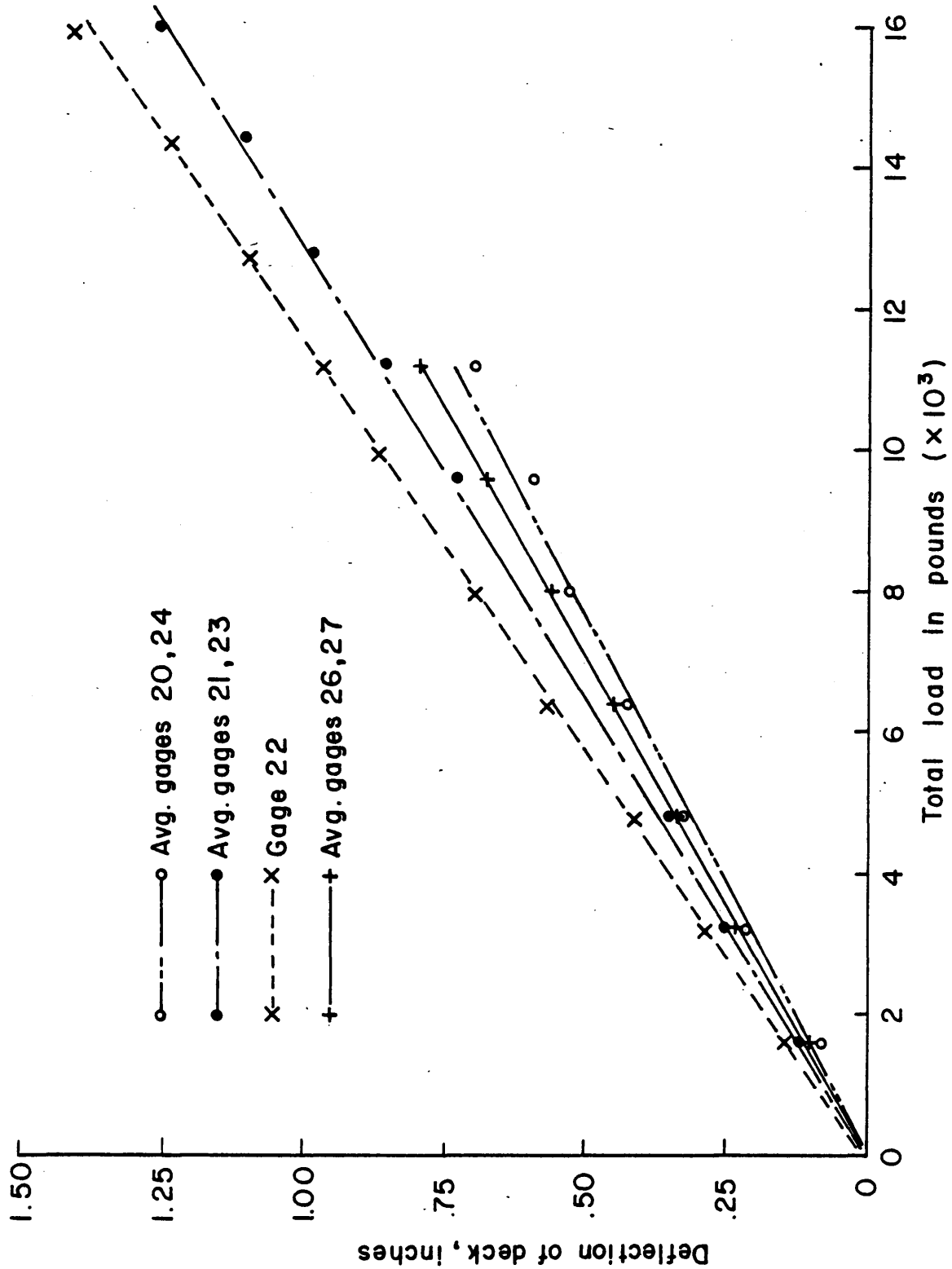


Figure 23. Deflections of the bridge for ultimate load test.

Gages 14, 16, 30, and 31 were read at each load increment for comparative purposes. The data from these gages are included in Figure 24. As seen from the curves, the relationship between the strain and load appears to be bilinear for all gages. A break occurs at the 6,400-lb load for gage 30 and at the 8,000-lb load for the other three gages. Strains from gages 14 and 16 are comparable due to their locations and reflect the differences in strains between the middle (loaded) and outside (unloaded) girders. The fact that the maximum strain difference was only 17% between the two girders attests to the efficient lateral transfer of load from one girder to another through the cover plate and concrete wearing course.

The distribution of the strain across the section (top, center, and bottom) of the lower chord is depicted by the data from gages 30, 31, and 14. As mentioned previously, strain gages mounted on the surface of a chord or web member did not measure the average strain in the member, and comparisons with theoretically computed values were expected to show considerable variance. The data from gage 30 appear to converge at a higher load with those for the other two gages, but it is doubtful if a completely uniform strain would be achieved over the cross section of the member within a reasonable working stress level.

The maximum recorded strain of gage 16 was 1,967  $\mu\text{in/in}$  at a load of 16,000 lb. Thus it appears that the lower chord of the middle girder was stressed to something over 15,000 psi when the ultimate load was reached. In view of an ultimate tensile strength in excess of 100,000 psi for the GRP strands making up the web and chord members, the likelihood of a tensile failure in a stranded member is quite remote.

#### Acoustic Emission Measurements

A total of only 63 counts were recorded when the bridge failed. The first count was noted at a load of 4,800 lb, with a fairly uniform rate of emissions occurring until the ultimate load was reached. A pause of approximately 2 minutes was made in the load application at each of the increments of 1,600 lb to permit deflection and strain readings. During these pauses, several emissions were recorded, which indicated that cracks or fiber breakage in the composite material were continuing at the constant load. There was no opportunity to ascertain the length of time the counts may have continued. Surprisingly, the acoustic emission sensor did not pick up the "big bang" when the horizontal stiffener failed. Apparently, the acoustic attenuating properties of the composite material precluded the transmission of the strain energy from the end of the outside girder to the center of the middle girder. Had the sensor been mounted near the failure location on the west girder, many thousands of counts would have accumulated from the failure of the stiffener. Therefore, it may be concluded that the AE counts recorded during the load test detected only the relatively small damage in the center part of the middle girder.

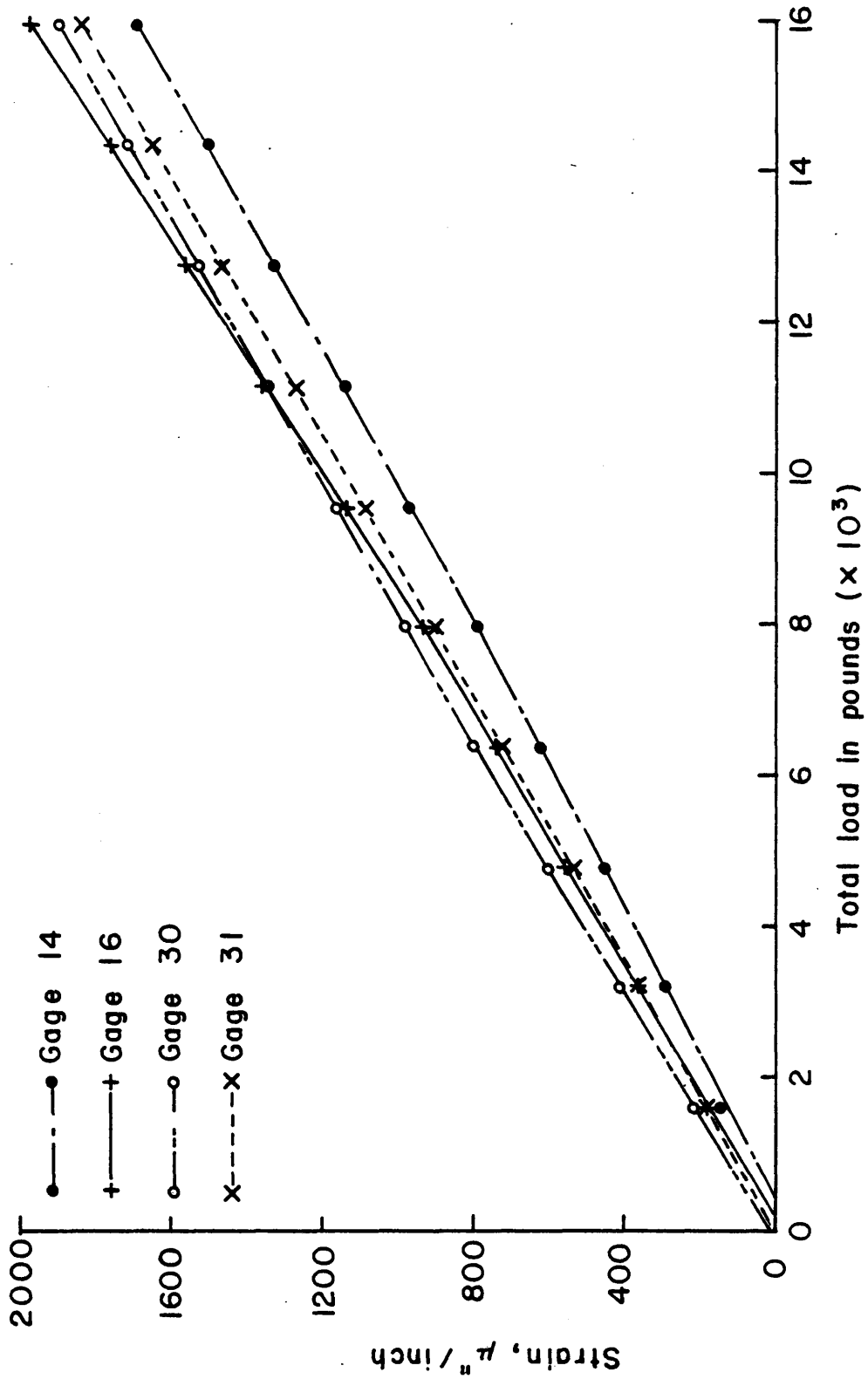


Figure 24. Strains in two lower chords for ultimate load test.

## ANALYTICAL STUDIES

Vertical displacements, strains, and stresses in the elements of the bridge were computed for various static load configurations by means of a finite element model. The model was defined with elements and nodes suitable for solution by the computer code Engineering Analysis Systems, ANSYS. ANSYS was developed by Swanson Analysis Systems, Inc. of Houston, Pennsylvania. The computations were performed on a Prime computer at the University of Virginia. All elements in the finite element model were assumed to be linearly elastic and all deformations were assumed to conform to the restrictions of small strain theory. A complete description of the geometry, elements, node and material properties used for constructing the model are included in Appendix B. The arrangement of loads and a description of assumed constraints for the elements are also included in Appendix B.

Comparison of the experimental results with the numerical solutions are shown for deflections in Table 6 and for strains and stresses in Table 7. The locations of deflection indicators and strain gages are shown in Figure 6. The identification of the nodes and elements in the model is provided in Appendix B. Three load series are discussed as representative of the data obtained from the three load arrangements used for the cyclic studies. In each case, the calculated values are compared with the experimental data obtained from the first static load reference test for their particular load series.

Comparisons of Deflections

The differences in the load arrangements of series 1 and 2 compared with series 6 required different analytical approaches for the two cases. In series 1 and 2, the load spreader beam was parallel to the horizontal stiffeners attached to the flanges of the girders and, therefore, it did not induce bending in the stiffeners about their transverse axes. However, for series 6 the spreader beam was perpendicular to the horizontal stiffeners and did induce considerable transverse bending in the stiffeners of the (loaded) middle girder. The outside girders were loaded only by the shear force and counterclockwise couples transmitted through the cover plate and wearing course from the middle girder. While some bending of the plates and stiffeners undoubtedly occurred in the outside girders due to the couple, it was considered negligible compared with the bending caused by the load applied directly to the middle girder. Because of these conditions, the analyses for load series 1 and 2 did not consider bending of the horizontal stiffeners in any of the girders, but for load series 6 bending of the stiffeners was considered in the middle girder only. A second behavioral consideration of the bridge involved the rotational resistance of the horizontal stiffeners about their own longitudinal axes due to the action of the vertical web stiffeners. While the degree of restraint was unknown, it was obvious that some condition between fixed and free existed for the members.

TABLE 7

## Comparison of Experimental and Analytical Deflections

Gage	Node	Experimental in	Analytical Solution							
			Degree of Rotational Constraint, Percent of Fixed							
			0,		40,		50,		60,	
		in	% Diff.	in	% Diff.	in	% Diff.	in	% Diff.	
Deflections for load series 1										
2	28	.125	.186	+ 49	.136	+ 9	.124	0	.112	- 10
3	23	.113	.185	+ 64	.134	+ 19	.123	+ 9	.111	- 2
4	30	.183	.302	+ 65	.219	+ 20	.200	+ 9	.182	0
5	15	.177	.306	+ 73	.221	+ 25	.202	+ 14	.183	+ 3
6	25	.172	.297	+ 73	.215	+ 25	.197	+ 15	.179	+ 4
Deflections for load series 2										
2	28	.242	.290	+ 20	.206	- 15	.186	- 23	.165	- 32
3	23	.226	.288	+ 27	.205	- 9	.185	- 18	.164	- 27
4	30	.151	.348	+130	.250	+ 66	.226	+ 49	.201	+ 33
5	15	.162	.352	+117	.252	+ 55	.228	+ 41	.203	+ 25
6	25	.137	.346	+152	.248	+ 81	.225	+ 64	.200	+ 46
Deflections for load series 6										
2	28	.190	.348	+ 83	.260	+ 37	.239	+ 26	.216	+ 14
3	23	.173	.278	+ 61	.197	+ 14	.177	+ 2	.156	- 10
4	30	.289	.566	+ 96	.424	+ 47	.388	+ 34	.353	+ 22
5	15	.310	.575	+ 85	.429	+ 38	.392	+ 26	.357	+ 15
6	25	.278	.443	+ 59	.313	+ 13	.281	+ 1	.249	- 10

Computations were made for several presumed constraints based on a percentage of the rotation which would occur for each stiffener if the member were completely free to rotate with the flange plate without any torsional resistance from the vertical stiffeners.

The results of the computations are shown in Table 7 for series 1. These data show that an excellent agreement with the experimental values was achieved when a theoretical constraint of 60% fixed was applied to the horizontal stiffeners. It is apparent that the differences between the experimental and analytical values would change as the joints between the stiffeners and flanges or other elements in the structure were damaged due to cyclic load applications. For example, the differences for gage 4 between the first reference load test at 0 cycles and the last reference load test at 500,000 cycles changed from 0% to -13% for the assumed 60% restraint condition. For the 50% assumed restraint, the agreement was better, with a difference value of -4%.

The results of the computations for load series 2 also are shown in Table 7. The difference between the experimental and analytical results are much larger for load series 2 than for load series 1. The larger differences are attributed to the upward buckling of the deck over the northern half of the bridge. The elastic buckling of the deck was not considered in the analytical model, so differences in the numerical values were expected; particularly for gages 4, 5, 6, 7, and 8, which were located in the buckled region of the bridge. A graphical comparison of the experimental and analytical data is shown in Figure 25 for the deflections of the lower chord along the centerline of the middle girder for the assumed 60% fixed rotational constraint of the horizontal stiffeners. The deflection profile deduced from the several known experimental data points clearly shows the effect of the buckled deck when compared with the deflection profile from the analytical solution.

The lower portion of Table 7 presents the results for the deflections from load series 6. As noted in the previous discussions for load series 1 and 2, the rotational constraint of the horizontal stiffener was also influential in minimizing the differences between the experimental and analytical results. The best overall agreement for the values appears to be between the 50% and 60% restraint conditions. It is also interesting to note that the predicted lower chord deflections for the loaded (middle) girder, gages 2 and 4, were always greater than the measured values for the cases shown. On the other hand, the predicted deflections for the unloaded (outside) girder, gages 3 and 6, varied from greater to lesser than the measured values as the degree of constraint increased.

#### Comparison of Strains and Stresses

Comparisons between the strains measured with bonded electrical strain gages and those computed from the mathematical model are tabulated in Table 8. The values for stresses were computed directly from the

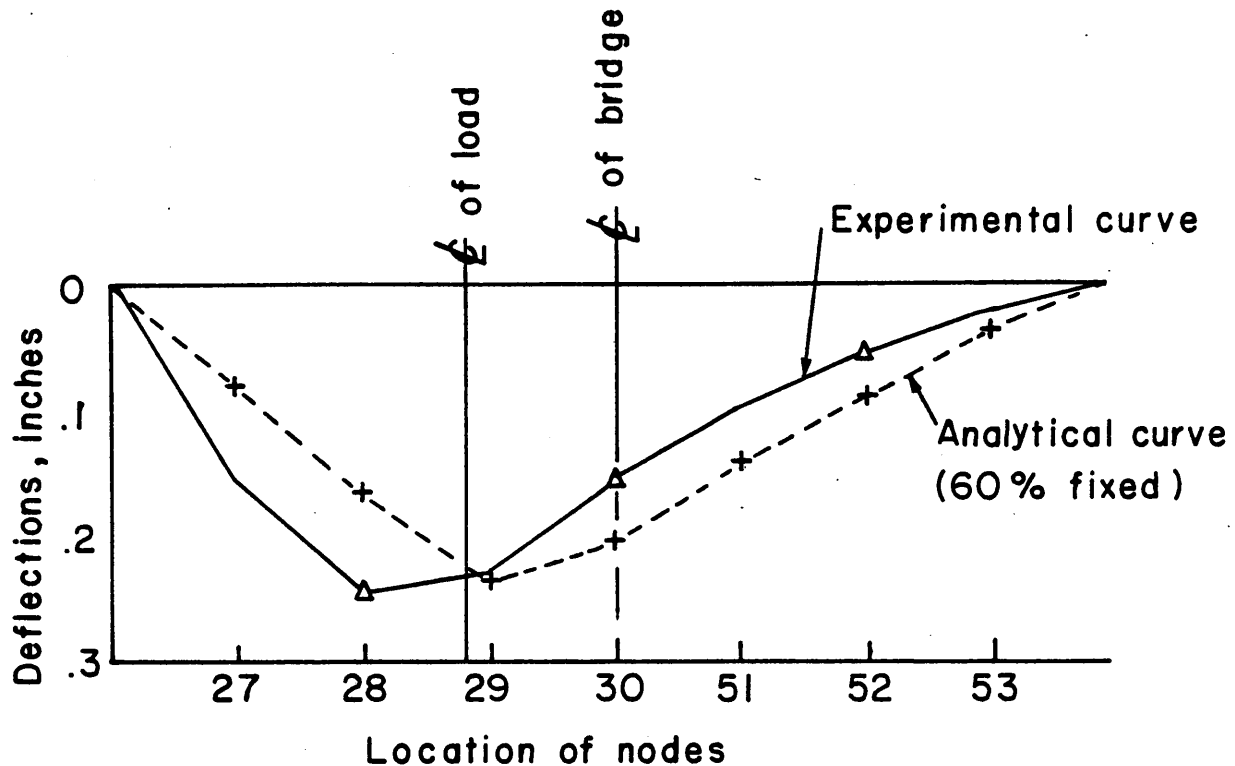


Figure 25. Comparison of experimental and analytical deflections for load series 2.

from the measured and computed values of strains by the relation axial stress = elastic modulus times strain with an elastic modulus of  $7 \times 10^6$  psi for these members. The values for the gages mounted on the deck plates were considered unreliable and are, therefore, not included in the table. It was expected that there would be large differences between the theoretical and measured strains because the elements upon which the gages were mounted underwent both axial and flexural deformations. The nature and magnitude of the flexural distortions, while believed to be small, were unpredictable, variable, and generally indeterminate.

Gages 1 through 7 in Table 8 were mounted on diagonal web members. All of these members were subjected to primary axial tensile forces for all load arrangements and secondary couples as might be transmitted through the joints between members. The theoretical strains were larger than the measured values by variable amounts until the 60% fixed restraint was used for load series 1 and 50% for load series 2. Load series 6 produced random differences for all restraint conditions. As noted in the discussion of the deflections, the best agreement between the experimental and analytical strain results was with an assumption of 60% fixed condition for the horizontal stiffeners.

TABLE 8

## Comparisons of Experimental and Analytical Strains and Stresses

Gage	Element	Experimental		Analytical							
		Strain, $\mu\text{in/in}$	Stress, ksi	Degree of Rotational Constraint, Percent of Fixed							
				0		40		50		60	
		$\mu\text{in/in}$		$\mu\text{in/in}$	%	$\mu\text{in/in}$	%	$\mu\text{in/in}$	%	$\mu\text{in/in}$	%
Strains and stresses for load series 1											
1	46	449	3.1	743	+ 65	544	+ 21	498	+ 11	451	0
2	54	488	3.4	764	+ 57	560	+ 15	512	+ 5	464	- 5
3	47	459	3.2	761	+ 66	557	+ 21	510	+ 11	462	+ 1
5	48	494	3.5	886	+ 79	633	+ 28	578	+ 17	523	+ 6
6	49	545	3.8	904	+ 66	650	+ 19	594	+ 9	539	- 1
7	50	490	3.4	783	+ 60	580	+ 18	537	+ 10	495	+ 1
13	30	431	3.0	403	- 6	291	- 32	266	- 38	241	- 44
15	34	466	3.3	406	- 13	294	- 37	269	- 42	243	- 48
16	35	370	2.6	456	+ 23	333	- 10	306	- 17	278	- 25
30*	31	329	2.3	450	+ 37	328	0	301	- 9	274	- 17
Strains and stresses for load series 2											
1	46	562	3.9	993	+ 77	698	+ 24	630	+ 12	558	- 1
2	54	694	4.9	1,020	+ 47	711	+ 2	641	- 8	568	- 18
3	47	604	4.2	1,014	+ 68	708	+ 17	638	+ 6	565	- 6
5	48	630	4.4	1,210	+ 92	875	+ 39	788	+ 25	698	+ 11
6	49	777	5.4	1,241	+ 60	894	+ 15	806	+ 4	714	- 8
7	50	394	2.8	804	+104	640	+ 62	595	+ 51	549	+ 40
13	30	697	4.9	803	+ 15	571	- 18	514	- 26	456	- 35
15	34	760	5.3	810	+ 6	575	- 24	518	- 32	459	- 40
16	35	681	4.8	750	+ 10	545	- 20	495	- 27	443	- 35
30*	31	537	3.8	745	+ 39	542	+ 1	493	- 8	441	- 18
Strains and stresses for load series 6.											
1	46	553	3.9	588	+ 6	338	- 40	273	- 51	210	- 62
2	54	719	5.0	1,387	+ 93	1,058	+ 47	980	+ 36	890	+ 24
3	47	648	4.5	1,193	+ 84	886	+ 37	814	+ 26	729	+ 12
5	48	570	4.0	653	+ 15	380	- 33	316	- 45	246	- 57
6	49	817	5.7	1,481	+ 81	1,115	+ 36	1,027	+ 26	935	+ 14
7	50	623	4.4	603	- 3	355	- 43	302	- 52	244	- 61
13	30	533	3.7	763	+ 43	540	+ 1	486	- 9	428	- 20
15	34	676	4.7	972	+ 44	727	+ 7	668	- 1	604	- 11
16	35	441	3.1	986	+123	738	+ 67	677	+ 53	615	+ 39
30*	31	426	3.0	756	+ 77	535	+ 26	481	+ 13	426	0

\* Average strain for gages 30, 31, and 14.

The manner in which the lower chord elements were formed from a multipath source of strands contributed to a nonuniform strain in the element adjacent to a lower chord joint. (See Appendix A for diagrams of the winding patterns for the web and chord elements.) An investigation of strain variation over the cross section of a lower chord element was conducted by means of bonded strain gages 30, 31, and 14, which were located on the top, middle, and bottom surfaces of the chord, respectively. From this it was determined that the maximum strain was more than twice the minimum strain for some loads and that the ratio of maximum to minimum strains varied with the magnitude and location of the load on the bridge deck. These results indicated that the measured strains on the chord members could differ considerably from an average strain across the section. When comparing the average experimental strain measurements of gages 30, 31, and 14 with the analytical values based also on an average strain, the agreement among the results shown in Table 8 is quite good for load series 1 and 2 with a 40% restraint condition and for load series 6 with a 60% restraint condition.

The values for axial tensile stress in Table 8 are shown corresponding to the experimental strains. Several noteworthy observations may be made relative to the development of stress in the members of the bridge.

1. All stresses were similar in magnitude for a given test load, whether the member was a diagonal web or lower chord.
2. The rank order of stress magnitude among the members remained the same for each of the load series.
3. Web element 49 (gage 6) was the most highly stressed member for all of the load series.

In summary, it appears that the distribution of stresses in the stranded members was reasonably uniform and that the stress relationship between the members did not change radically with a change in the arrangement of the load on the structure.

## SUMMARY OF FINDINGS

The investigation of the fatigue characteristics of the bridge due to several arrangements and magnitudes of cyclic loads provided the following information.

1. A total of 1.62 million cycles of load were applied to the bridge.
2. A crushing failure of a support element early in the test program was believed to be caused by damage to the bridge prior to the fatigue loading. After repair, the support element performed satisfactorily throughout the remainder of the fatigue test.
3. Cracks developed in some of the adhesive joints between horizontal stiffeners and the flange plates of the girders. These cracks slowly increased in length and width as the numbers of load cycles increased. Changes in the sizes of the cracks were randomly distributed throughout the three girders and appeared to act as stress relievers for the joints as loads were transferred from a highly stressed element to one stressed at a lower value. In this regard, the overall bridge appeared to be highly redundant internally.
4. As a consequence of the progressive cracking of the stiffener-plate joints, the elastic deflection of the bridge under load increased progressively, which reflected a degradation in the stiffness of the structure.
5. There was evidence of viscoelastic creep under load which also contributed to the measured deflections of the girders. However, upon removal of the load, the viscoelastic behavior was more apparent from observations of the deflection (and internal strain) recovery of the bridge over a period of time. Residual deflections and strains were observed after periods of relaxation following the removal of the loads but absolute magnitudes were not quantified.
6. The polymer concrete wearing course performed excellently throughout the cyclic load tests. No surface cracks were observed, and tensile strength tests of the bond at the interface of the cover plate gave no indication of bond degradation. The tensile strengths of the polymer concrete and the interfacial bond exceeded 400 psi.
7. The deck assembly (flange and cover plates and polymer concrete wearing course) underwent slight elastic and viscoelastic buckling under compressive stresses. The magnitude of (upward) buckling was particularly evident with nonsymmetrical loading.

8. Lateral load transfer was satisfactory for all load arrangements, with no indications of distress to any components of the bridge.
9. A theoretical analysis of elastic deflections and strains of the bridge was conducted by means of a finite element code ANSYS. In view of the uncertainties associated with material properties and joint deformations, the agreement between the experimental and theoretical values was considered to be satisfactory.

#### CONCLUSIONS AND RECOMMENDATIONS FOR DESIGN AND RESEARCH

The considerable experience accumulated over the period since the inception of the bridge study in 1975 has provided test data and insights relative to criteria for the design of prototype structures and some of the needs for additional behavioral information.

On the plus side, the assembled bridge exhibited unexpected toughness throughout the laboratory tests and the field tests, and when moved from one site to another. Damage of the support stiffeners due to handling was easily and satisfactorily repaired. The relatively light weight of the structure permitted handling with a minimum of equipment. The tensile strength of the elements constituting the structure was considerably in excess of the applied or design loads. The geometric configuration of the triangular-trussed girders with flanges coupled with bonded cover plates provided lateral and torsional stability to the bridge. While the abrasive resistance of the polymer concrete surface was not evaluated, the integrity of the concrete and the development of the bond at the surface of the cover plate were satisfactory. The size used for the web and chord members in the girders resulted in a relatively uniform and therefore efficient distribution of stresses throughout the members for the condition of symmetrical loading.

On the negative side, the elastic deflections of the bridge were excessive for design loads. Deflections due to viscoelastic creep also occurred, and while they were partially recoverable in time with the removal of load, the creep would contribute to residual deformations in the bridge. Adhesive joint failure due to progressive cracking under high cyclic loading could eventually cause a functional failure via excessive deflections or a collapse of the bridge due to separation of members at the joints. The number of cycles which the bridge could withstand at the design load is unknown, but is believed to be larger than several million.

Recommended changes in the basic design to improve the strength and stability of the individual girders include the following:

1. Replace the hollow-tube stiffeners at the supports with solid rods to prevent crushing.
2. Increase the effectiveness of the mechanical connection at the end of the horizontal stiffeners to reduce cleavage stresses in the stiffener-plate adhesive joint.
3. Provide cross web diagonals in the truss panels to accommodate negative shear forces generated by non-symmetrical loads.
4. Replace the glass-fiber strands in web and chord members with strands of a higher modulus material such as aramid or carbon.

Recommendations for additional investigations and modifications to the current bridge configuration include the following:

1. Conduct parametric studies of the geometric configuration of the girders to minimize deflections due to dead and live loads. The ANSYS computer code and the behavioral model of the current bridge would provide a starting point for such an analysis.
2. Extend the computational model from a simply supported girder to a member which is continuous over several supports. Based on the results of an analysis of the girder, fabricate and test a reduced scale model of the member to verify the analysis.
3. Study the effectiveness of using a "cored" pultruded flange section for the girder in lieu of the flat plate used in the current structure.

## REFERENCES

1. McCormick, F. C., "Experimental Bridge Girder of Reinforced Plastic," Transportation Engineering Journal of ASCE, Proceedings of the American Society of Civil Engineers, Vol. 101, No. TE1, February 1975.
2. \_\_\_\_\_, "Study of a Trussed Girder Composed of a Reinforced Plastic," VHTRC Report No. 75-R6, Virginia Highway and Transportation Research Council, Charlottesville, Virginia, August 1974, 40 pp.
3. McCormick, F. C., and H. Alper, "Further Studies of a Trussed-Web Girder Composed of Reinforced Plastics," VHTRC Report No. 76-R16, Virginia Highway and Transportation Research Council, Charlottesville, Virginia, November 1975, 78 pp.
4. McCormick, F. C., "Modification Studies for a Bridge Girder of Reinforced Plastics," VHTRC Report No. 77-R5, Virginia Highway and Transportation Research Council, Charlottesville, Virginia, July 1976, 29 pp.
5. \_\_\_\_\_, "Laboratory and Field Study of a Pedestrian Bridge Composed of Reinforced Plastics," Bridge Engineering, Vol. 2; Transportation Research Record 665, September 1978, pp. 99-107.
6. \_\_\_\_\_, "Field Study of a Pedestrian Bridge of Reinforced Plastic," VHTRC Report No. 86-R21, Virginia Highway and Transportation Research Council, Charlottesville, Virginia, December 1985.



APPENDIX A

BRIDGE FABRICATION DESCRIPTION AND MATERIALS

574

### Fabrication of Girders

All fabrication information was taken verbatim from Reference 5, "Laboratory and Field Studies of a Pedestrian Bridge Composed of Reinforced Plastic"

The fabrication of TTG-WC closely paralleled that of TTG-13 with some modifications. These modifications included the replacement of wooden bolts with brass bolts in the flange-to-stiffener connection, the elimination of positioning pins in the joint between the stiffeners and the lower chord connectors, and sandblasting of all bonded surfaces. A corrosion resistant metallic bolt was used to provide more strength than that available from the wooden bolts. The 6 mm (1/4 in.) diameter pins were omitted from the lower chord connector because they were determined to be structurally ineffective and were not required for the assembly procedure. All mating surfaces which were to be bonded with an epoxy adhesive were sandblasted to assure removal of the release agent used in the manufacture of the pultruded products. A No. 1 silica sand was used in a sandblaster at an air pressure of 275 Pa (40 psi) to clean the surfaces of plates and stiffeners. This operation was time-consuming but provided a better bond surface than previously obtained by belt sanding. The manpower requirement for the winding operation of each of the three girders was approximately the same (six man-hours) as that for TTG-13.

### Assembly of Bridge

The three identical girders were assembled to form the prototype structure by bonding a common cover plate (6 mm [1/4 in.] thick) to the top flange plate and by connecting the lower chords with strands of glass-impregnated roving. It was essential that the adhesive joint between the girder flange and cover plate should be as free from voids as possible to develop the shear strength required for the integrity of the compression element for the bridge. Previous experience in bonding large surface areas during the assembly of TTG-8 (see reference 2) provided an indication of the difficulty in achieving a void-free joint. The two primary contributing factors in the assembly problem was the inherent warpage of the pultruded plates and the bending or distortion of the top plate resulting from the attachment of stiffeners and tension strands during the fabrication of the girder. While both of these factors were individually small, there was some concern that the distortion could be eliminated in order to provide contact over most of the plate area within the 0.075 mm (0.003 in.) thickness required by the glue line. It was obvious that a normal clamping force would be required to hold the surfaces together while the adhesive cured. Because of the large areas involved and the time required to complete the joint, an epoxy that cured at room temperature was selected for the adhesive.

In view of the above considerations, steel beams were placed transversely beneath all three girders and supported at the ends so that the top plate of each girder rested directly upon the steel beam. Careful leveling of the beams and alignment of the girders longitudinally achieved a reasonably rectangular and planar configuration for the overall surface for the bridge. The cover plates, 1.2 m (4 ft.) wide, were cut to lengths of 2.1 m (7 ft.) in order to eliminate all longitudinal joints and to simplify the bonding procedure. Four cover plates were therefore used to cover the entire bridge area. Prior to coating adhesive on both plates, the surfaces were cleaned thoroughly with an acetate solvent. Positive contact between mating plate surfaces was achieved by applying C-clamps along the edges, bolting three clamping strips per cover plate, and applying pressure through an air bag over the center portion of the plate. Figure 12 shows a typical arrangement for bonding one of the cover plates. The supporting steel beams may be seen in the lower right of the figure. The air bag was in contact over the full width of the bridge along a strip slightly less than 1 m (3 ft.) wide. The adhesive was permitted to cure under pressure for at least five days at a room temperature 23°C (70°F). Inspection of the bonded joint after curing was made by visual observation around the edges of the plates and by scanning portions of the plates with an ultrasonic detector. The visual inspection revealed that most, but not all, of the peripheral joints were free of open cracks.

Several regions were selected for ultrasonic scanning which were either considered to be well-bonded or had a likelihood of improper bonds. The well-bonded regions included the central portions of the contact surfaces over which the air bag had been pressurized. The regions of questionable bonds were along the interior edges of the cover plates, the interior edges of the flange plates, and particularly the "corner" areas formed at the intersections of the joints in the flange and cover plates. As described previously, the inherent curvature in the respective plates and the inability to provide positive clamping along the interior edges of the cover plates during assembly raised some doubts as to the nature of the bonded joint in these areas. The ultrasonic inspection was made with a V-Scope, Model C-4960, manufactured by James Electronics of Chicago, Illinois, as shown in Figure 13. The V-Scope measured the time required for a high frequency audio wave to pass through the two plates and epoxy joint. Calibration of the instrument with a "good" joint and one with an extensive void established a well-defined measurement of the time delay due to the void. Approximately 50 points were surveyed along the joined edges of the plates. Nearly one-half indicated the presence of voids. However, the voids did not appear to extend beyond 75 mm (3 in.) from the edge of the plate. One point (at one of the corner intersections) strongly indicated a crack or a separation of the plates extending approximately 75 mm (3 in.) from the edge. None of the points checked with the V-Scope in the central regions of the plates (presumably well-bonded areas) showed any indication of voids or cracks. From the visual

inspections and ultrasonic surveys made of the bonded plates, the plate assembly procedure appeared to be successful even though it was tedious and required intermittent steps.

After the cover plate was bonded to the top plate of the girders, the entire structure was inverted and the lower chord connectors of parallel girders were tied together with strands of roving as described previously. This operation was quite simple and was completed within several hours. Figure 14 shows this operation. However, inverting the structure without exerting undesirable forces or distortion on the plates or chords required special efforts and fixtures. Wooden braces were attached throughout the bridge and movable wooden towers were built to act as supports for the structure as it was rotated.

#### Instrumentation

The bridge was instrumented with electrical resistance strain gages to monitor the deformation of various diagonals, chords and plates. A total of twenty electrical strain gages (Micro Measurements CEA-06-250-UW-350) were bonded (epoxy, M-Bond AE 15) to the surfaces at selected locations to measure strains in various stranded elements and plates.

#### MATERIALS USED IN FABRICATION

The following materials were used for the fabrication of the girders.

1. Pultruded square tubes and plates were obtained from Morrison Molded Fiberglass Company, Bristol, Virginia. All materials were grade Extren 500.
2. Glass-fiber reinforcement was obtained from Owens Corning Fiberglass Company, Toledo, Ohio. Type 30, E glass roving was used for winding all tensile elements.
3. Polyester resin, Type E 477, used to impregnate the glass roving was also obtained from Owens Corning Fiberglass Company.

Small quantities of MEKP were used as the catalyst to provide a gel time of approximately 50 minutes.

4. Bonded joints between pultruded sections and plates with epoxy adhesives furnished by Morrison Molded Fiberglass Company (Kit 502) and H. B. Fuller Company, St. Paul, Minnesota, (Resiweld FE7004).

APPENDIX B

DESCRIPTION OF THE FINITE ELEMENT MODEL OF THE BRIDGE

1/4-and 1/2-Bridge Models

A mathematical model of the bridge was described by the following characteristics for use with the finite element computer code ANSYS. Descriptions of the elements and nodes for 1/4-and 1/2-bridge models are given in Figures B-1 and B-2. Each node was permitted the number of degrees of freedom (DOF) as indicated for its associated component with the exception of certain nodes which were constrained to represent the conditions of symmetry or known boundary conditions. The excepted nodes are specified for each of the load models in Figures B-3 through B-6. The values for the elastic moduli shown for the elements represent the best estimates available. Considerable uncertainty remains for the values of the stranded members (web diagonals and lower chords) due to the variability in winding tension and shrinkage strains resulting from the cure cycle of the resin matrix. In addition, the "effective" modulus of the vertical web stiffener assembly is a function of the fit of the connecting pins and lower chord connector.

Elements

1. Component: plate and deck  
 ANSYS type: STIF 43  
 No. of nodes: 4  
 DOF per node: 6:  $u(x)$ ,  $u(y)$ ,  $u(z)$ ,  $\phi(x)$ ,  $\phi(y)$ ,  $\phi(z)$   
 Modulus: 2,100,000 psi  
 Thickness: 1.25
  
2. Component: vertical web stiffener  
 ANSYS type: STIF 8  
 No. of nodes: 2  
 DOF per node: 3:  $u(x)$ ,  $u(y)$ ,  $u(z)$   
 Modulus: 841,000 psi (effective)  
 Area: 0.4375 in<sup>2</sup>
  
3. Component: lower chord  
 ANSYS type: STIF 8  
 No. of nodes: 2  
 DOF per node: 3:  $u(x)$ ;  $u(y)$ ,  $u(z)$   
 Modulus: 7,000,000 psi  
 Area:
 

E1 #28 = .0536 in <sup>2</sup>	E1 #32 = .0268 in <sup>2</sup>
#29 = .1608 "	#33 = .0804 "
#30 = .2948 "	#34 = .1474 "
#31 = .4020 "	#35 = .2010 "
  
4. Component: horizontal stiffener  
 ANSYS type: STIF 8  
 No. of nodes: 2  
 DOF per node: 3:  $u(x)$ ,  $u(y)$ ,  $u(z)$   
 Modulus: 2,300,000 psi  
 Area: .6875 in<sup>2</sup>

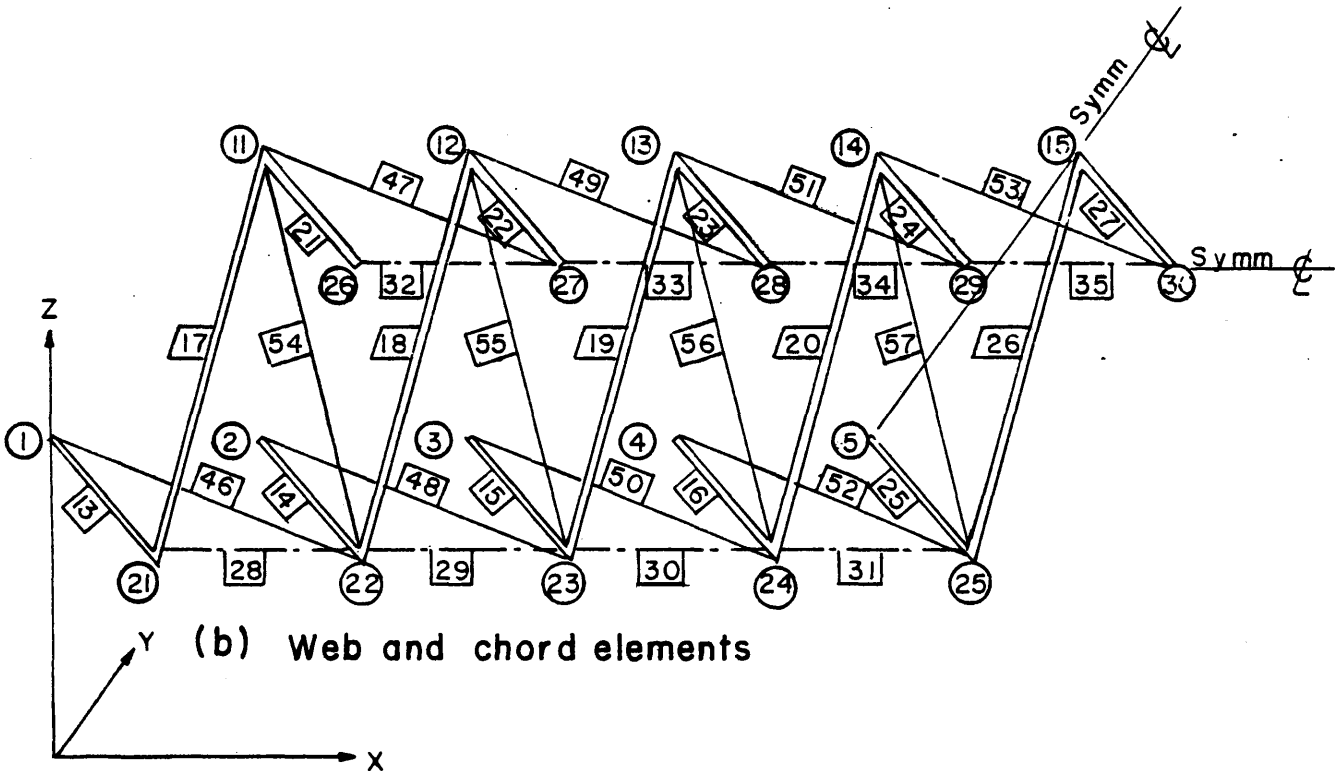
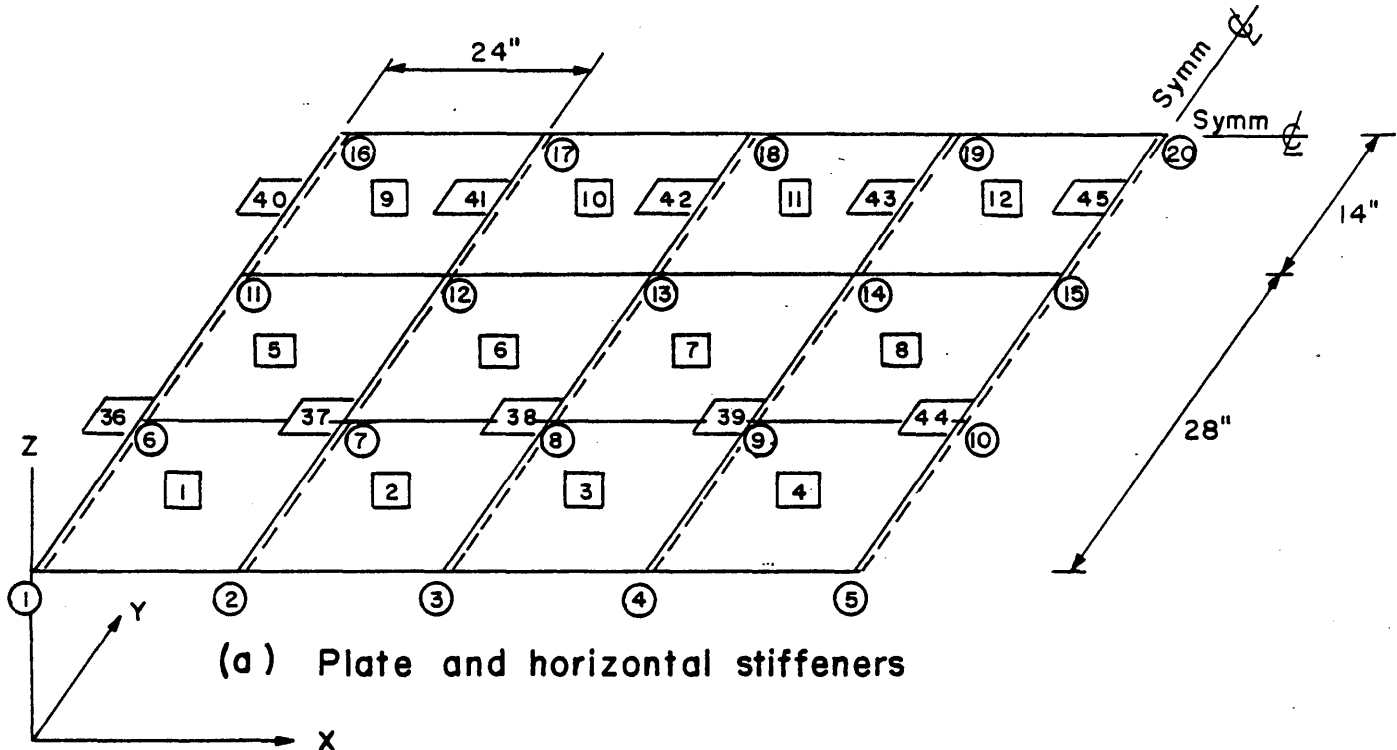


Figure B-1. Designation of elements and nodes for 1/4-bridge model (see Figure B-3 for key.)

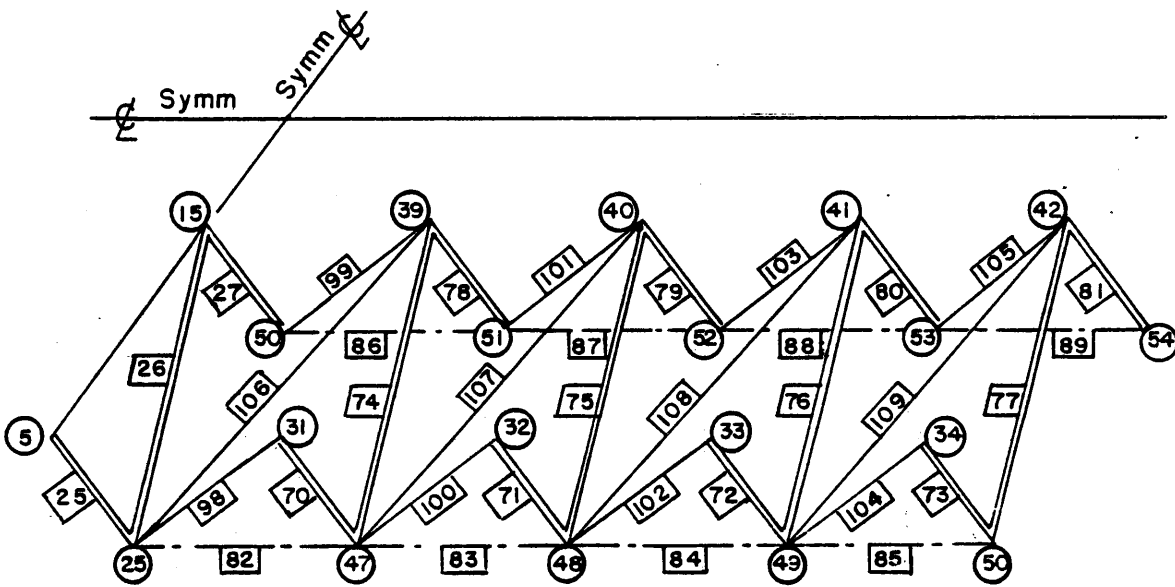
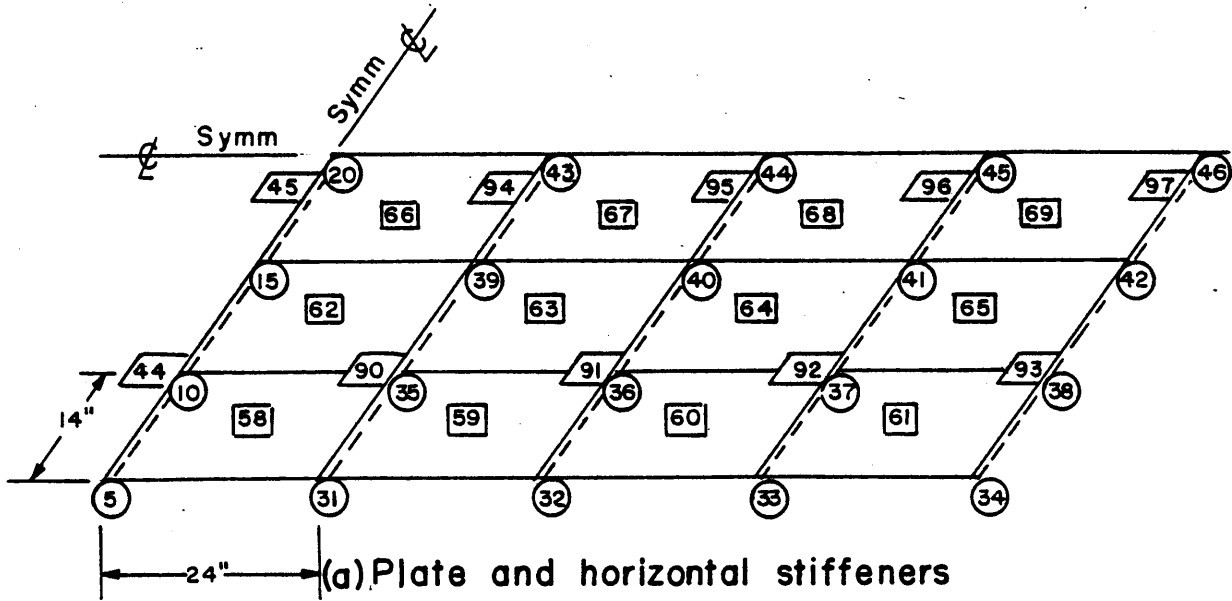


Figure B-2. Designation of elements and nodes to be added to Figure B-1 to form a 1/2-bridge model (see Figure B-3 for key.)

5. Component: diagonal chord  
 ANSYS type: STIF 10  
 No. of nodes: 2  
 DOF per node: 3: u(x), u(y), u(z)  
 Area: El #46, 47, 54 = .0804 in<sup>2</sup>  
       #48, 49, 55 = .0670 "  
       #50, 51, 56 = .0536 "

See Figures B-1 and B-2 for the location of the basic elements and nodes with respect to the geometry of the structure.

Additional elements used in load series 6.

6. Component: plate and deck (El. 58, 59, 60, 61)  
 ANSYS type: STIFF 43  
 No. of nodes: 4  
 DOF per node: 6: u(x), u(y), u(z),  $\phi(x)$ ,  $\phi(y)$ ,  $\phi(z)$   
 Modulus: 2,100,000 psi  
 Thickness: 0.75"
7. Component: horizontal stiffener  
 ANSYS type: STIF 4  
 No. of nodes: 2  
 DOF per node: 6: u(x), u(y), u(z),  $\phi(x)$ ,  $\phi(y)$ ,  $\phi(z)$   
 Modulus: 2,300,000 psi  
 Area: .6876 in<sup>2</sup>  
 Mom. of inertia:  $I_{yy} = I_{zz} = 0.2184 \text{ in}^4$

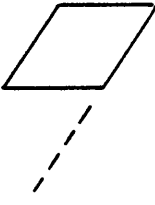
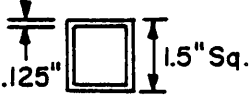
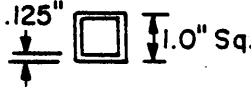
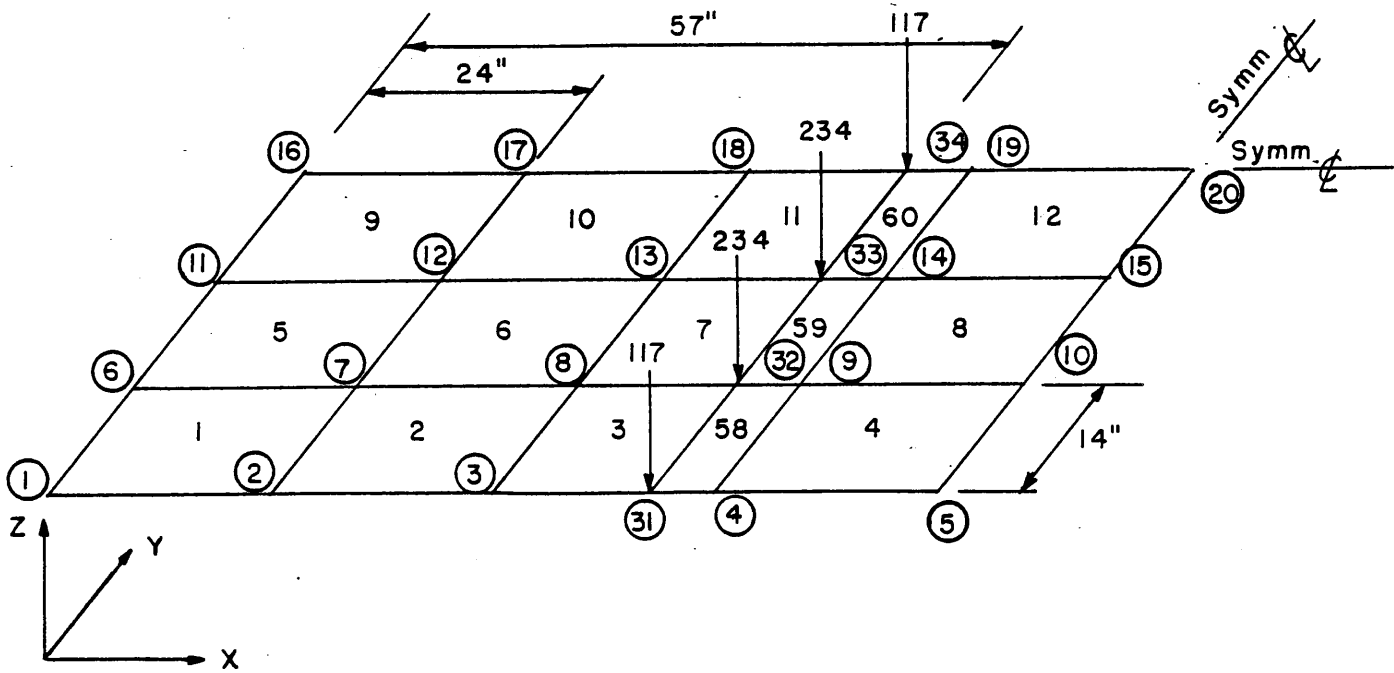
Symbol	Description	Cross section	Area, in <sup>2</sup>
	Plate	$t = 1.25''$	
	Horizontal stiffener		.6875
	Vertical web stiffener		.4375
	Lower chord		Varies
	Diagonal web		Varies

Figure B-3. Key to symbols for Figures B-1 and B-2.

#### Loading Models

Some variations were made to the basic model to accommodate the differences in the load applications. Because of the double symmetry of the load distribution in load series 1, the basic computational model used was the 1/4-bridge section shown in Figure B-1. The addition of 4 nodes and 3 plate elements with their appropriate degrees of freedom permitted the application of the loads at the actual locations on the deck as indicated by the nodal points shown in Figure B-4. Similarly, the double symmetry of the load distribution in load series 6 permitted the use of a 1/4-bridge section with no modifications to the basic model of Figure B-1. The load arrangement and constraints for load series 6 are shown in Figure B-5. The single symmetry of the load distribution in series 2 required the use of the basic model of the 1/2-bridge shown in Figure B-2. This model was modified as described for load series 1 and the results are shown in Figure B-6.

In all of the load models, concentrated forces were applied at the designated nodal points to represent the loads distributed along the length of the spreader beam. It was determined from several variations of the number and magnitude of loads that the number of load points finally selected introduced very little error in the computation for strains and deflections at locations away from the load. The precise distribution of the load applied to the deck was unknown in view of the flexural moduli and behavior of the steel beam and the deck of the bridge.

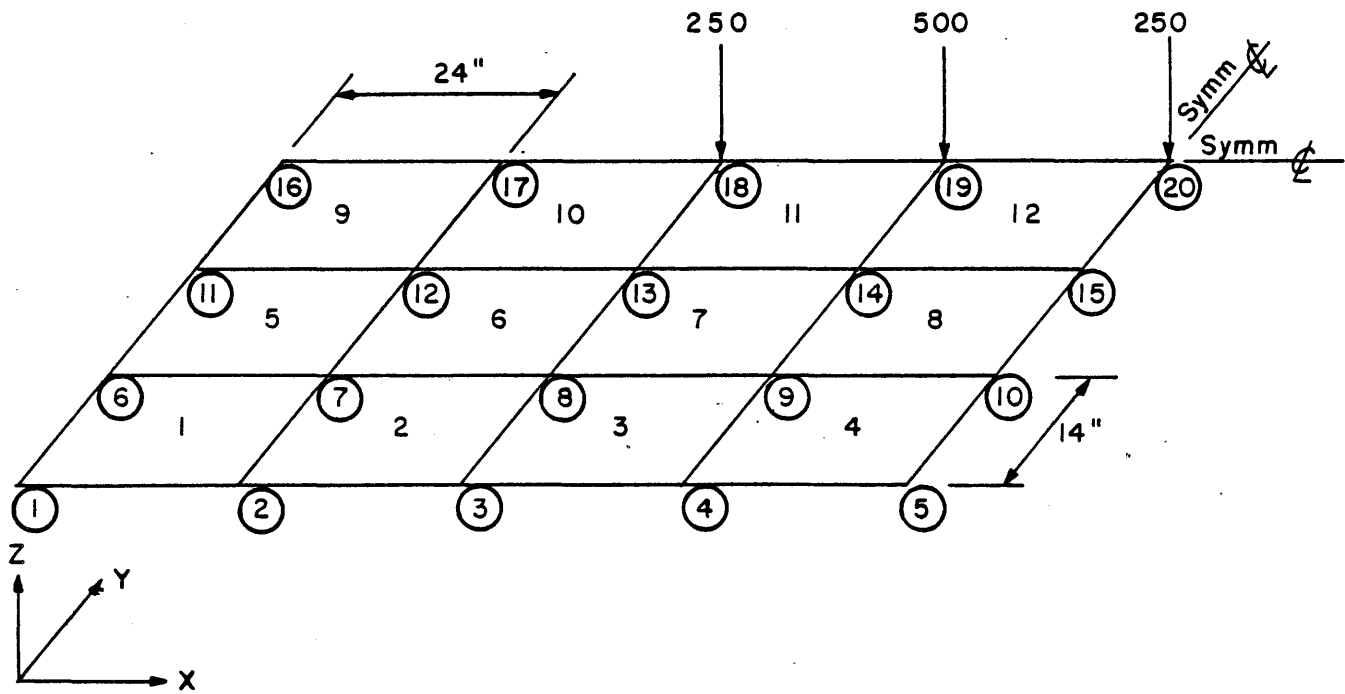


Total Line Load = 700 lb on 1/4 section. P/3 = 234 lb.

Constraints:

Nodes	1,6,11:	$u(x) = u(y) = u(z) = 0$
	16:	$u(x) = u(y) = \phi(x) = 0$
	5,10,15:	$u(x) = \phi(y) = 0$
	20:	$u(x) = u(y) = \phi(x) = \phi(y) = 0$
	17,18,19,34:	$u(y) = \phi(x) = 0$
	21,26,27,28,29:	$u(y) = 0$
	25:	$u(x) = 0$
	30:	$u(x) = u(y) = 0$

Figure B-4. Arrangement of loads for load series 1.



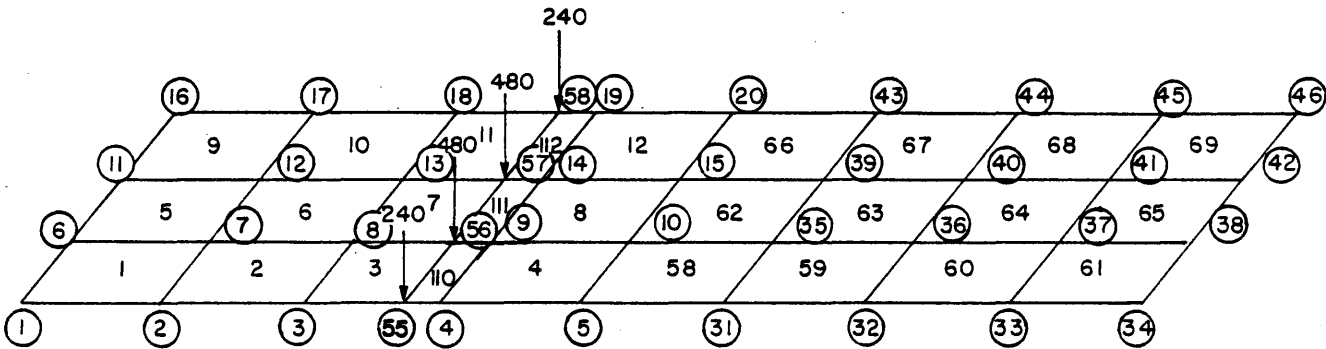
## Load Series 6

Total Line Load = 4,000 lbs.  $P/8 = 500$  lb,  $P/16 = 250$  lb.

## Constraints:

Nodes 1,6,11,31:	$u(x) = u(y) = u(z) = 0$
16:	$u(x) = u(y) = u(z) = \phi(x) = 0$
5,10,15,35:	$u(x) = \phi(y) = 0$
20:	$u(x) - u(y) = \phi(x) = \phi(y) = 0$
17,18,19:	$u(y) = \phi(x) = 0$
21,26,27,28,29:	$u(y) = 0$
30:	$u(x) = u(y) = 0$
25:	$u(x) = 0$

Figure B-5. Arrangement of loads for load series 6.



Total Line Load = 2,900 lbs. P/12 = 240 lb, P/6 = 480 lb.

Constraints:

- |                          |                             |
|--------------------------|-----------------------------|
| Nodes 1,11:              | $u(x) = u(y) = u(z) = 0$    |
| 6:                       | $u(z) = 0$                  |
| 16:                      | $u(y) = u(z) = \phi(x) = 0$ |
| 17,18,19,20,43,44,45,48: | $u(y) = \phi(y) = 0$        |
| 34,42:                   | $u(x) = u(y) = u(z) = 0$    |
| 38:                      | $u(x) = u(z) = 0$           |
| 40:                      | $u(x) = u(y) = \phi(x) = 0$ |
| 50,51,52,53,54:          | $u(y) = 0$                  |

Figure B-6. Arrangement of loads for load series 2.

